Doctor Dissertation

Study of Photo-Magnetic Effect and Spin-Lattice Relaxation on Shallow Donors in Silicon Using a SQUID Magnetometer

Michio Kondo

March 1987

Department of Material Physics
Faculty of Engineering Science
Osaka University

Abstract

Photo-magnetic(PM) effect is a change in magnetization which arises from spin reversal and change in the orbital diamagnetism associated with optical excitation and subsequent relaxation. The PM effect is one of optical processes which generally occurs in solid, however has little been reported so far. A SQUID magnetometer responds sensitively to a small and rapid change in magnetization. The aim of this paper is to study the PM effect observed in silicon using the SQUID magnetometer and to elucidate its origin.

Instruments have been constructed for observing the PM effect. Besides, the SQUID detection of the ESR has been developed for comparison with the PM effect. The PM effect in ruby has been demonstrated, and has been compared with the SQUID-ESR. It has been shown for ruby that photoirradiation produces a population change between Zeeman levels of the ground state and the PM effect gives information on spin-lattice and spin-cross relaxation processes similar to the ESR.

On shallow donors in silicon, it has been found for the first time that uncompensated n-type samples show the diamagnetic change in magnetization induced by extrinsic infrared(IR) light at liquid He temperatures. The samples used are in the low concentration region from 2.2×10^{16} to 3.2×10^{17} P/cm^3 where the donor states are isolated from each other. The IR light excites electrons of neutral donors D^o to the conduction band. Subsequently, the conduction electrons recombine with ionized donors D^+ and are captured by the neutral donors to form negatively charged donors D^-. Two possibilities are assumed for the origin of the PM effect observed: the depolarization of the donor

spins and the orbital diamagnetism of the D^- states. The observed quantities are the steady state amplitude and the half decay time of the magnetization change. These quantities depend on the temperature, the donor concentrations and the IR background(BG) intensity. Furthermore it has been found that a partial compensation prevents from occurrence of the PM effect.

In order to determine either of the two possibilities of the PM effect, the SQUID-ESR and the FIR photoconductivity have been observed. The former gives information on the spin depolarization of donors, and the latter gives that on the lifetime of the D^- state. These results have been compared with that from the PM measurement, and it is concluded that the depolarization of the donor spins is responsible for the PM effect, and the diamagnetism of the D^- states is excluded. The PM effect observed indicates that photocarriers yield two remarkable events in the donor spins: depolarization of the donor spins and decrease in the spin-lattice relaxation times. In a sample with 9×10^{16} P/cm^3 it has been observed that the spin polarization is decreased by 23 % and the spin-lattice relaxation time of 1 sec is shortened to 0.24 sec depending on the IR light intensity. These results observed are discussed on the basis of the rate equation proposed and the reasonable explanation is given.

Though the mechanism for the above two events has not been satisfactorily understood, it may be due to the spin exchange scattering of carriers by donors, otherwise may be due to the superexchange interaction between the donors through the D^- states.

Acknowledgments

This research problem was suggested by Professor Y. Nisida, and has been studied under his guidance. The author would like to acknowledge his generous encouragement and fruitful discussions.

The author would like to thank Emeritus Professor S. Narita for his helpful comments and suggestions.

The author also would like to thank Drs. M. Kobayashi and K. Muro for their useful suggestions.

The SQUID magnetometer was constructed with the assistance of Messrs. Y. Hikino and S. Ochi. The photomagnetic measurement was made with the assistance of Mr. K. Ebata. The FIR photoconductivity was measured with the assistance of Mr. T. Nakano. The SQUID-ESR measurement was made with the assistance of Mr. K. Mori. The compensated sample was prepared by Mr. H. Ono. The author expresses the particular appreciation to them.

Finally the author would like to thank Miss M. Yamada for her kind assistance in preparing the manuscript.

Contents

Chapter I .Introduction

1.Shallow Donor state and D^- state in Si

Substitutional impurities such as phosphorus in silicon introduce hydrogen like states, i.e., shallow donor states, in the forbidden energy gap. These states are described by the effective mass theory (EMT)[1] where the anisotropic effective masses (m_l=0.98 m_o, m_t=0.19 m_o) and the dielectric constant of Si (ε =11.7) are taken into account. The EMT is in good agreement with the experiment for the energy levels of excited donor states, while the central cell correction is necessary for the ground state which has non-vanishing amplitude of the wave function in the vicinity of the donor ion. At a small distance from the donor ion the central-cell potential is introduced to correct the EMT for the ground state. Silicon has six equivalent conduction band minima in the direction on the <100> axis in the Brillouin zone, and the donor states are expressed by the superposition of the Bloch states around the band minima. The central cell potential with a T_d symmetry lifts the six-fold degeneracy of the 1s-like state into the lowest singlet, the upper doublet and triplet. The ionization energy of the ground state is 45 meV which is obtained by the optical absorption spectra.

The electron spin resonance (ESR) experiment on the ground state of the shallow donor in Si has been studied extensively by several workers.[2-5] In the low concentration limit, the donor electron is completely isolated from each other, and the ESR spectrum consists of a doublet (line width~ 3 G, separation ~

42 G) for phosphorus doped sample. The doublet occurs by a hyperfine interaction between donor electron and P^{31} nucleus with spin 1/2.

The spin-lattice relaxation was studied by Feher et.al..[2,3] The relaxation time T_1 depends on donor concentration $N(D^O)$, temperature T, magnetic field H. Below 1 x 10^{16} P/cm^3, T_1 is independent of the concentration and is of the order of 10^3 sec. The relaxation rate $1/T_1$ varies approximately as T and H^4 above 8000 G, which indicates the direct phonon process. On the other hand, above 1 x 10^{16} P/cm^3 up to 3 x 10^{17} P/cm^3, the relaxation time varies in the wide range from 10^3 sec to 10^{-4} sec depending on the concentration. The relaxation rate $1/T_1$ varies as T, but independent of the magnetic field.

Feher et.al. found another interesting phenomena[2]: reduction in the spin-lattice relaxation time induced by light illumination. The measurement was made on the sample with 7 x 10^{15} P/cm^3 which has the long relaxation time of 2 x 10^3 sec at 1.25 k and at 3200 G without the infrared background(IRBG) light. In the presence of the IRBG light (0.5 eV < $h\nu$ < 0.66 eV), the relaxation time is reduced to 25 sec. Though it was explained that the reduction in the relaxation time may be due to the spin-exchange scattering of the conduction electrons with the donor electrons, further study has not been attempted. This phenomenon is intimately related to the present work as mentioned later.

With increasing the donor concentration, it is known that the donor cluster is formed[4]. Below a concentration of 1 x 10^{18} P/cm^3, however, the clusters are isolated from each other, i.e., the impurity band conduction does not occur yet. This region is

called a low concentration region.

When the extrinsic IR light($h\nu < E_g$) is illuminated on the sample at low temperature, some of photoexcited electrons in the conduction band is captured by neutral donors, which results in the generation of the D^- state. The D^- state is described by Chandrasekhar type wave function[6] analogous to the H^- state[7]. The binding energy of the D^- state $E(D^-)$ is given theoretically as 0.0555 Ry^* where Ry^* is the effective Rydberg energy. The existence of the D^- states in Si was experimentally confirmed by the FIR photo-conductivity[8-9], and the experimental value of $E(D^-)$ =1.7 meV was determined for phosphorus doped silicon, which is in good agreement with the theory. The concentration dependence[10] of the absorption spectrum of the D^- state indicates that the D^- state is isolated from neighboring donors below 5 x 10^{14} P/cm^3, and D_n^- compleces are formed above 1 x 10^{15} P/cm^3. The D_n^- compleces mean that an excess electron is trapped by n donors jointly. The isolated D^- state has a large electron orbit of 85 A due to the small binding energy, where the orbital radius $R(D^-)$ is calculated from the relation $R(D^-) = h/(2\ m^*\ E(D^-))^{1/2}$. For the D_n^- complex the orbital radius cannot be estimated by this simple relation. The ground state of the D^- state is considered to be spin singlet, and the D^- state with spin triplet has not been found experimentally.

The D^- states are generated by the IR light, and accordingly after the light is turned off the D^- states are annihilated by various relaxation processes: thermal excitation and FIR photoexcitation to the conduction band followed by the electron capture

of the ionized donors D^+, and the hopping of the excess electron of the D^- state to the neighboring D^o state followed by the recombination with D^+. At a low temperature the thermal excitation to the conduction band can be neglected, and the most dominant process is considered to be the hopping. The decay time of the D^- state due to the hopping was measured by Norton[11] using a transient photoconductive measurement. The experimental detail will be presented in ChapterV . The obtained decay time is about 150 μ sec at 1.5 K on the sample with 8.5 x 10^{15} P/cm^3.

2. Photo-Magnetic(PM) Effect in Si

A photo-magnetic (PM) effect is a change in magnetization which is induced by photo-irradiation[12-14]. As mentioned above the light illumination of the sample produces the reduction in the spin-lattice relaxation time of the neutral donors as well as the formation of the D^- states. Then we had following questions. Does not the polarization of donor spins deviate from its thermal equilibrium value in the presence of the IR light ? In addition, can we measure the orbital diamagnetism of the D^- states ? Both are expected to produce the PM effect. We have attempted to observe these phenomena using a SQUID magnetometer which responds sensitively for a small and rapid change in magnetization . In our preliminary observation,[38] it was found that the extrinsic IR illumination induces a diamagnetic change in magnetization on the sample with 9×10^{16} P/cm^3 at 1.7 K and at 750 G. After the illumination is turned off the magnetization returns to the thermal equilibrium value with a half-decay time of a few second. Moreover both the signal amplitude and the half decay time are decreased by the IRBG illumination.

The sample magnetization is described as

$$Mz = N(D^O) \frac{\beta^2 H_O}{k T_S} - N(D^-) \frac{\beta^2 H_O}{(m^*/m_O)^2 E(D^-)} + M_b , \qquad (1)$$

where $N(D^O)$ and $N(D^-)$ are the concentration of the neutral donors D^O and the D^- state, respectively, β is the Bohr magneton, H_O the static magnetic field, T_S the spin temperature, k the

magneton, H_o the static magnetic field, T_s the spin temperature of the donor electrons, k the Boltzmann factor, and M_b the bulk magnetization of silicon crystal. The positive sign implies the paramagnetism. In Eq.(1) we assume that the magnetic moment of a donor electron is a Bohr magneton and each D^- state is isolated from other donors. The first term in the right hand side of Eq.(1) is the contribution of the spin polarization of neutral donors and the second term is that of the orbital diamagnetism of the D^- states. The contribution of the spin polarization and the Landau diamagnetism of the photo-electrons is assumed to be negligible, because their steady-state numbers is very small. In the absence of the extrinsic light, $N(D^-)=0$ and T_s is equal to the sample temperature. In the presence of the light, the following reactions occur in the sample as shown in Fig. 1.

(i) $D^o + h\nu \rightarrow D^+ + e^-$ (photoexcitation of the donor electron)

(ii) $D^+ + e^- \rightarrow D^o$ (capture by the ionized donor)

(iii) $D^o + e^- \rightarrow D^-$ (capture by the neutral donor)

(iv) $D^- + D^+ \rightarrow 2D^o$ (recombination of the D^- and D^+)

(v) $D^o\uparrow + e^-\downarrow \rightarrow D^o\downarrow + e^-\uparrow$ (spin exchange scattering with the conduction electron.)

The arrows $\uparrow$ and $\downarrow$ denote spin direction. The spin temperature T_s should deviate from the lattice temperature T_L if the donor spin reversal occurs by any way in the reactions above. In addition the formation of the D^- states is taken into account. Consequently the magnetization change is expected to appear.

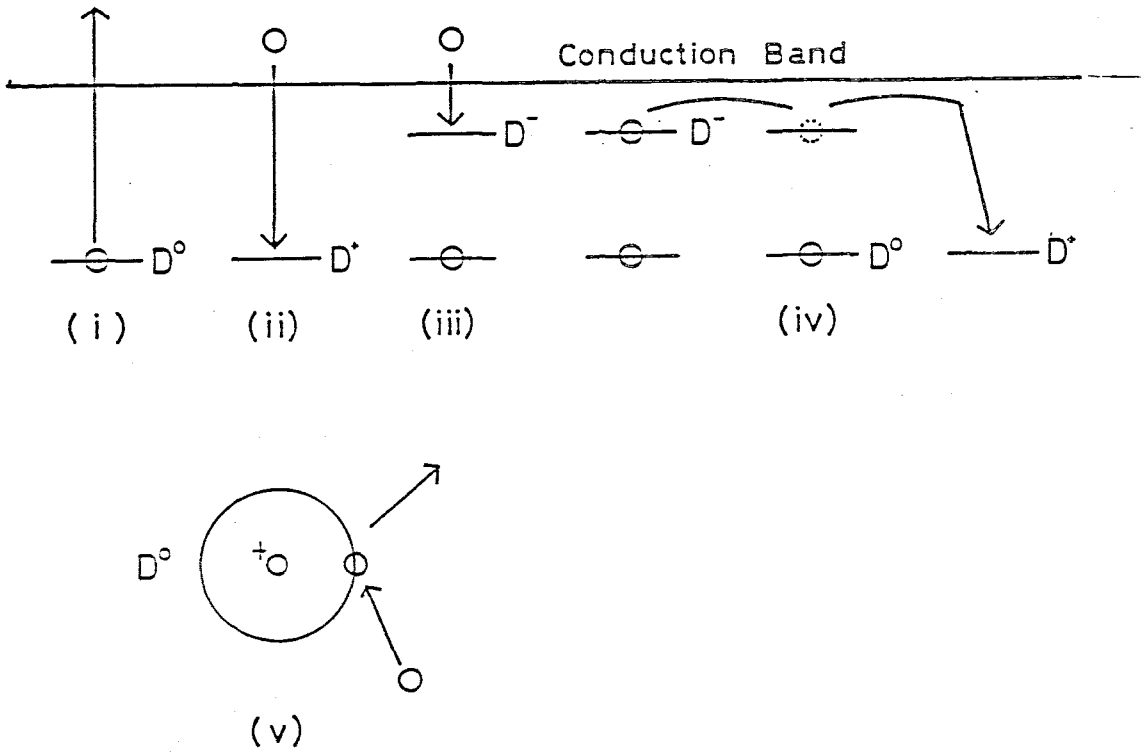

Fig. 1

Various reactions induced by photo-excitation in Si doped with shallow donors.

(i) extrinsic photoionization of D^{o}

(ii) recombination of an electron with D^{+} to form D^{o}

(iii) capture of an electron by D^{o} to form D^{-}

(iv) D^{-}-D^{+} recombination via hopping to adjacent donor sites

(v) spin-exchange scattering of an electron associated with a spin reversal of donor electron

3. Aim of This Paper

As mentioned above the PM effect on shallow donors in semiconductor has not been found before, and we assume the two possibility for the origin of the PM effect: spin depolarization of neutral donors; and orbital diamagnetism of the D^- states. The aim of this paper is to elucidate the characteristics and the origin of the PM effect.

For the study of the PM effect and the ESR on shallow donors in Si, we have developed the new experimental method using a SQUID magnetometer. As a test of the instruments, the PM and the ESR measurements are made on a paramagnetic system of ruby at first, which is described in ChapterⅡ. In ChapterⅢ the characteristic features of the PM effect in silicon are presented at first. Observed quantities, the signal amplitude and the half decay time, are described in each section, and then their dependence on the temperature, the background light and the donor concentration are presented. Finally, the PM effect for the FIR laser excitation is presented. The D^- concentration $N(D^-)$ is expected to be decreased because the D^- electron is excited to the conduction band by the FIR light, and therefore the sample magnetization may be changed according to Eq.(1). In order to clarify the origin of the PM effect, we made a SQUID-ESR measurement on the same sample as used in the PM measurement, which is described in ChapterⅣ. The SQUID-ESR can measure only the contribution of the donor spins but not the orbital diamagnetism of the D^- states. The observed results are compared with the PM ones, and the correlation between the PM effect and the ESR is

presented. In ChapterV the FIR photoconductivity is observed for comparison with the Norton's work on the lifetime of the D^- state. In ChapterVI we presents the discussion on the origin and the mechanism of the PM effect based on the whole experimental results, and propose a phenomenological explanation in terms of a rate equation approximation.

Chapter II .Instrumentation

The SQUID is a new sensor using the Josephson effect, and various applications have been attempted[12-23]. A measuring instrument of magnetization using the SQUID which is called a SQUID magnetometer has the following characteristics: 1)high sensitivity; 2)high precision; and 3)fast response. The characteristic 1)is superior to a conventional torque method or an ac method in the measurements of a small sample at a weak magnetic field[19]. The characteristic 2) means that the absolute value of magnetization can be simply and precisely measured[18] by the SQUID system. We have attempted for applying the characteristic 3) to observe the kinetics of magnetization. The magnetization is changed by applying external influences : rf magnetic field and photo-irradiation. The former is NMR[22-23] and ESR[23], and the latter is the PM effect.

1.Instruments for PM Measurements

1-1.Construction of Instruments

First, the design and the performance of the SQUID magnetometer using an rf SQUID are described in this section. The conceptual scheme is shown in Fig. 2. The pick-up coils L_1 and the SQUID input coil L_2 form a superconducting loop, and L_1 is located in a uniform and stable magnetic field.

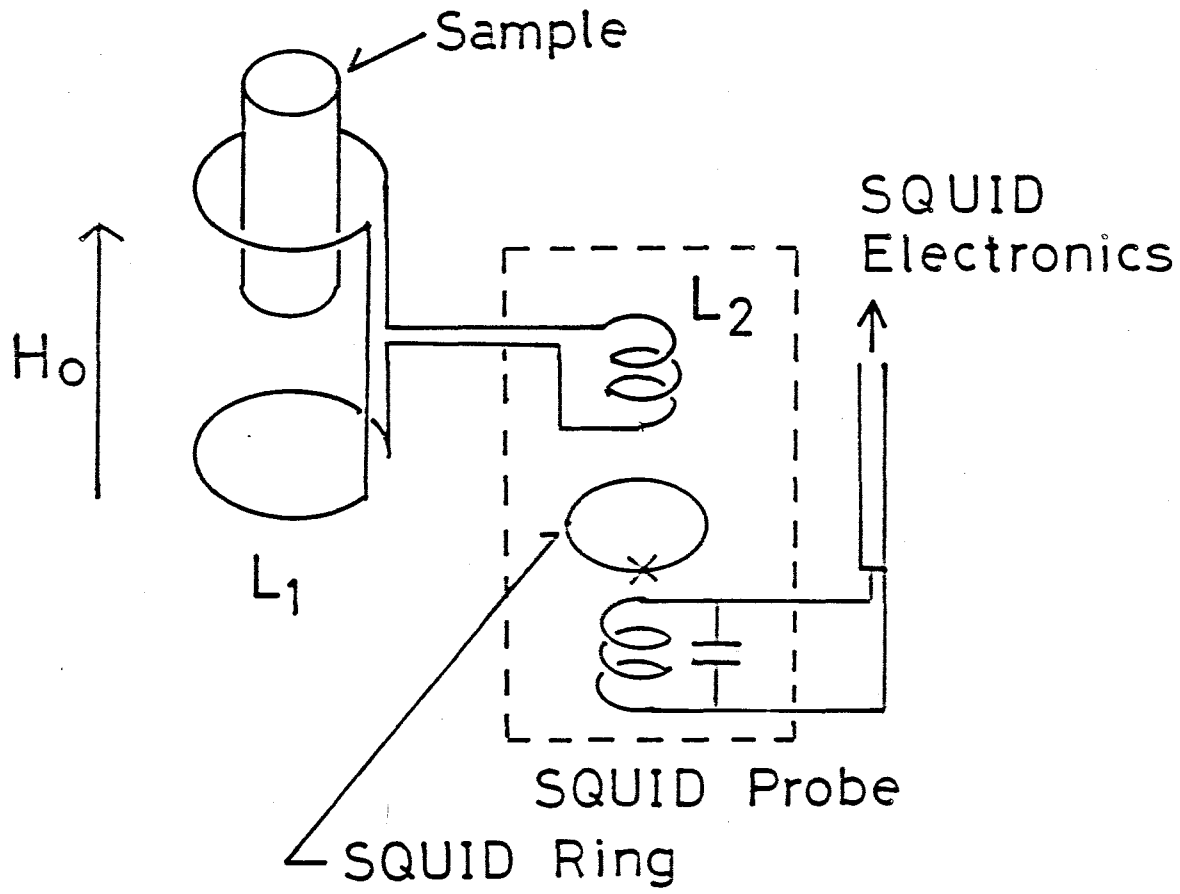

Fig. 2

Scheme for measuring magnetization using a SQUID sensor.

L_1: pick-up coils, L_2: input coil of a SQUID probe.

A superconducting current induced by the magnetization of the sample produces a magnetic flux on the SQUID ring. The flux is converted to the voltage signal by a flux locked loop in the SQUID electronics. The voltage converted is proportional to the sample magnetization.

When the external magnetic flux is applied to one of the pick-up coils , a screening current is induced so as to conserve the total magnetic flux inside the superconducting loop, and a flux proportional to the applied flux is transferred to the SQUID ring. The SQUID electronics operates to convert the magnetic flux to the voltage signal. The principle of the SQUID is reviewed in Ref.(15). Since a pair of pick-up coils are wound in opposite direction (astatically) with each other, a uniform fluctuation of the magnetic field produces no net current in the loop. When a sample is moved into one of the pick-up coils from far, the supercurrent proportional to the sample magnetization is induced. The construction of the SQUID magnetometer is based on the previous work[18] as shown in Fig. 3. A pair of 10-turns pickup coils are wound astatically on a Cu pipe with 10 mm diameter using 0.14 mm Nb wire. The pick-up coils L_1 are connected to the input coil L_2 in a SQUID probe as shown in Fig. 2. The inductance of the pick-up coils is matched with that of the SQUID input coil which is 2 μ H.

A static field, H_o, is supplied by a superconducting magnet operated in the persistent current mode, and the magnetic flux is trapped in a 13 mm i.d. Nb pipe. The available maximum field was about 1KG in the present apparatus. Even though the magnet is operated in the persistent current mode, the flux creep produces drift of the order of 10^{-10} G per sec. which generates a noise in the SQUID magnetometer.

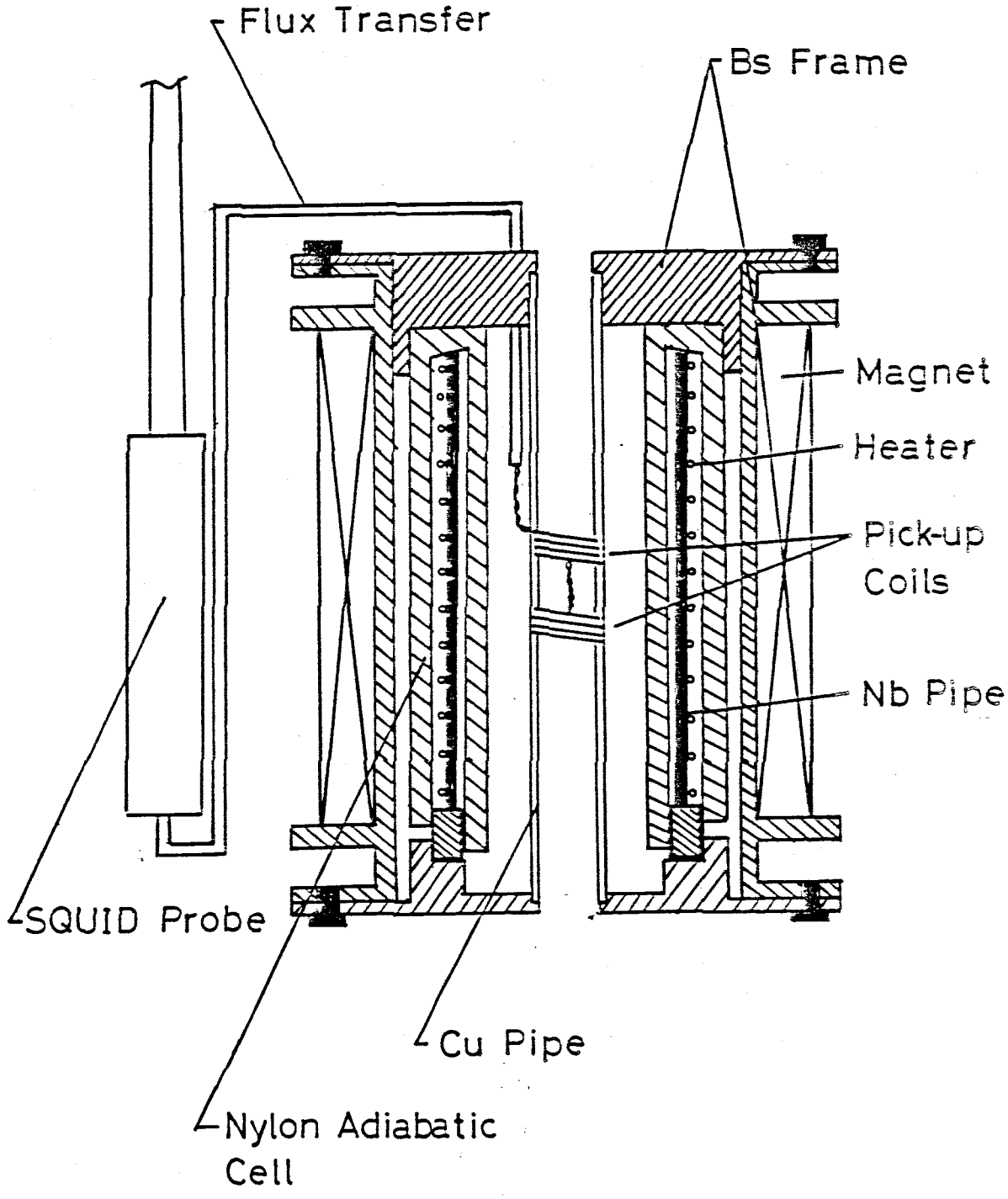

Fig. 3

Main portion of the SQUID magnetometer. The equipment is immersed into liquid He bath.

Non-zero resistance of the magnet wire at a welding point produces a gradual decay of the persistent current. If the resistance is 10^{-9} Ω and the inductance of the coil is 1 H, the decay time of the flux is 10^{9} sec which corresponds to 32 years. Accordingly the Nb pipe is used to provide a completely stable magnetic field. The Nb pipe also shields the pick-up coils from an external magnetic noise. In order to trap the magnetic flux inside the Nb pipe, the pipe is held in the normal state by heater wires wound noninductively on the pipe. After the pipe is made superconducting, only extremely small currents flow on the pipe to maintain the field, and the flux creep of the Nb pipe can be neglected. The Nb pipe was covered by a nylon plastic cell. When the pipe is heated, evaporated He gas thermally insulates the pipe from outer liquid He, and decreases loss of liquid He. In addition, the pick-up coils, the Nb pipe and the magnet are supported rigidly on the same brass frame to reduce noise due to their relative motion. The SQUID probe and the electronic controller are SHE 330 system. It has a response time of 0.2 msec which is limited by a feedback circuit.

An absolute calibration of the system was made by using a test solenoid with the same dimensions as a sample or by using a standard sample with known susceptibility. The SQUID output of 1 Φ_o corresponds to the magnetic moment of 6.5 x10^{13} spins in unit of Bohr magneton at the " x 100 " mode, where $\Phi_0 = 2.07 \times 10^{-7}$ G cm^2, the flux quantum.

The overall noise in flux Φ_N is 5×10^{-2} Φ_o at a magnetic field of 440 G and at a measuring bandwidth of 3 KHz. The main source of the noise may be attributed to the mechanical vibration

of the pick-up coils in the small inhomogeneity of the static field. The noise is decreased to 1/10 at temperatures below the λ -point of liquid He. The noise level gives a limit in the minimum detectable magnetic moment, which is evaluated to be about 3.3×10^{12} spins in the sample. In this work the size of the sample was $3 \times 3 \times 5$ mm^3.

In the measurements of the PM effect a sample is located at the inside of one of the pickup coils and is illuminated by exciting light. When the excitation is turned on, the change in the sample magnetization is induced and is sensed by the SQUID magnetometer. In the measurements the amplitude of the SQUID response and the waveform of the temporal change in magnetization are recorded in a digital transient memory.

The experimental arrangement for observation of the PM effect in ruby is shown in Fig. 4. An exciting light from a 250 W high pressure mercury lamp is focused by a quartz lens and is led to a sample in a cryostat through glass fibers. An optical filter is placed in the light path to remove unnecessary light. The light is gated by a mechanical shutter or a chopper. The light guide around the sample is made carefully. The outer pipe is made of a Cu pipe with 5 mm i.d., and the sample is supported by a 99.999% Cu rod with 5 mm o.d.. In the portion of the outlet of the fiber to the sample, the quartz light guide is used to reduce the reflection loss of the Cu light pipe, and a high purity quartz (sprasil) is used near the sample to avoid a spurious signal due to the magnetic impurities.

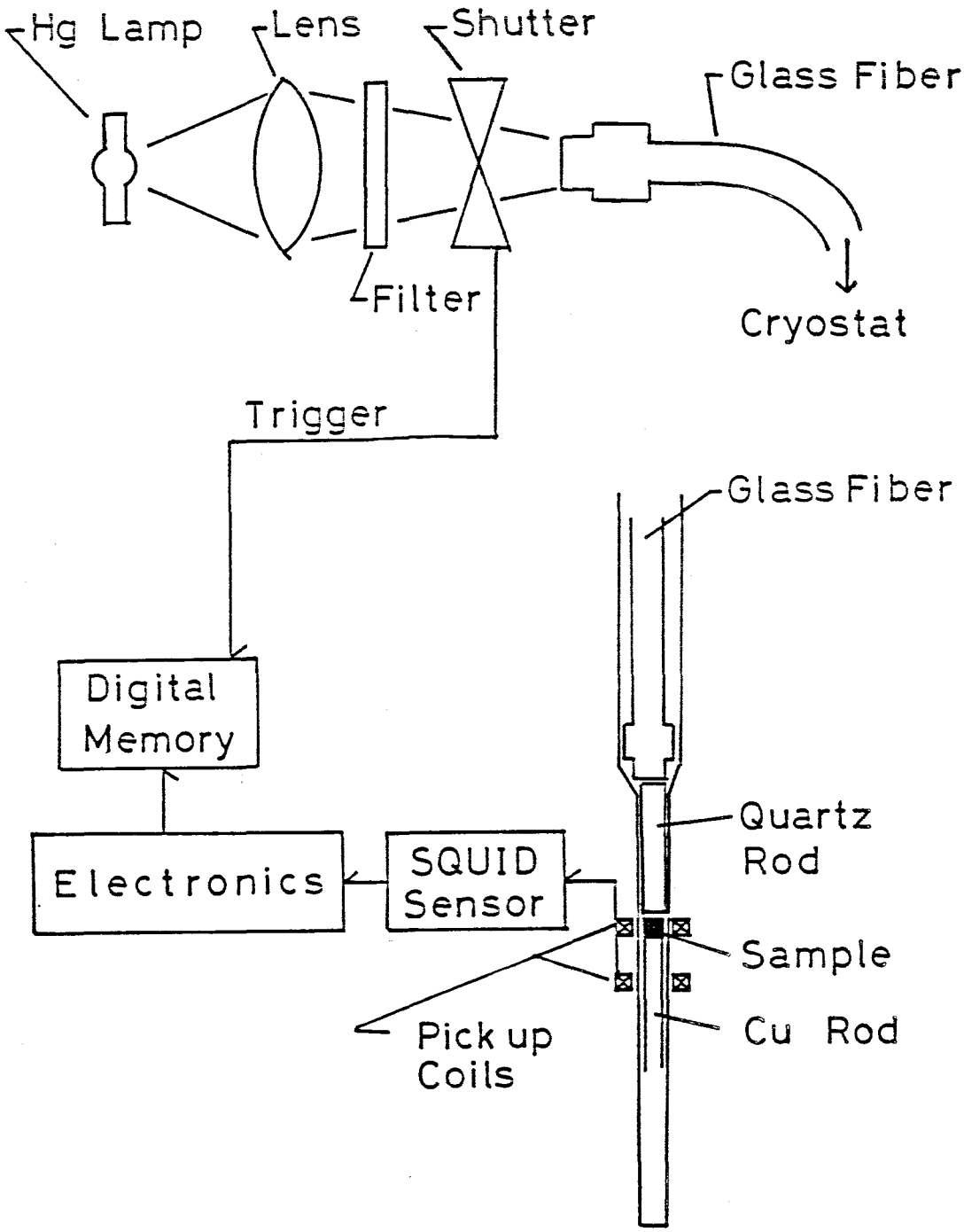

Fig. 4

Schematic diagram of the instruments for measuring the PM effect of ruby.

When the exciting light is turned on the temperature of the equipments around the sample will rise owing to the absorption of the light, and a slight amount of paramagnetic impurities in the material produces a ghost signal, which cannot be separated by the measuring system because the SQUID senses total change in magnetization. Accordingly the high purity and nonmagnetic materials are used for the equipment around the sample. Similarly, since the sample temperature is inevitably raised by photo-excitation, the sample and the equipment near the sample are in direct contact with liquid He to prevent from heating.

1-2. Demonstration of PM Effects

In this section the results for ruby are presented. The energy levels of Cr^{3+} in ruby are shown in Fig. 5-(a). The ground state of Cr^{3+} in ruby is S=3/2 and the Zeeman level splitting[24] at θ = 0° and at θ =90° are shown in Fig. 5-(b), where θ is an angle between the static magnetic field H_o and the c-axis. Typical traces on the samples doped with 0.05 mol% Cr^{3+}, are shown in Fig. 6 for the case that θ =0° and θ =90° at 4.2 K and at 300 G. At θ =0° the waveform consists of two components. One is diamagnetic with a shorter relaxation time τ_1 of 0.23 sec after the photo-excitation and another is paramagnetic with a longer relaxation time τ_2 of 0.65 sec. On the other hand at θ =90° the signal consists of a single diamagnetic component with a shorter relaxation time of 0.23 sec after the photoexcitation.

Table 1 shows the dependence of the relaxation time on Cr^{3+} ion concentration, temperature and the angle θ . On the sample

with 0.01 mol% Cr^{3+} ions the feature is essentially the same as the 0.05 % sample, while on the sample with 0.3 mol% Cr^{3+} ions the longer relaxation time is not observed but only the shorter is observed even at $\theta = 0°$. The shorter relaxation times have almost the same value in this concentration region.

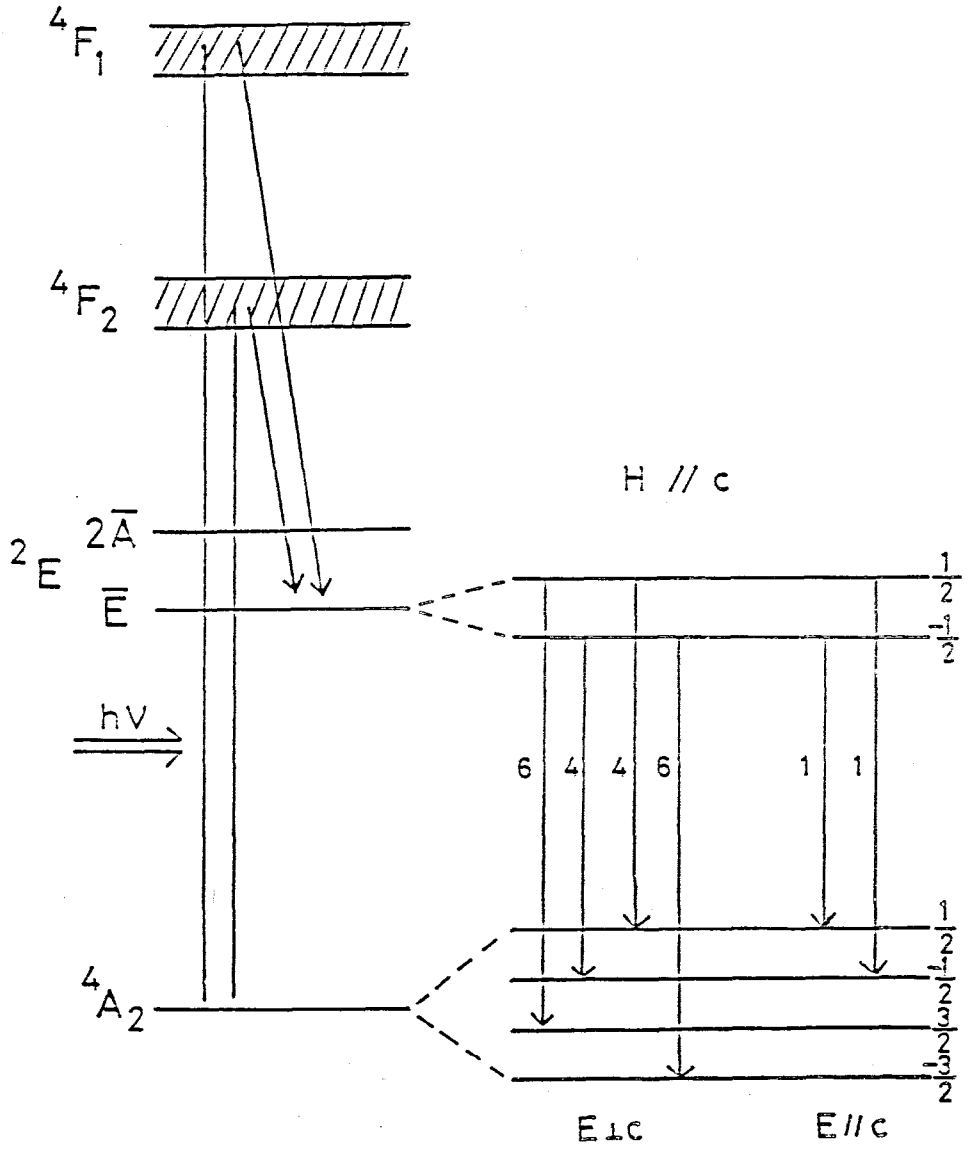

Fig. 5-(a)

Energy levels of ruby and the relative radiative transition rates in the magnetic field at θ =0° .(See Ref.(28)) The angle θ is taken between the magnetic field and the c axis of crystal. The transition rates are shown in the case that the electric field of the light is parallel and perpendicular to the c axis.

The vertical arrows in the figure indicate the excitation and subsequent relaxation processes.

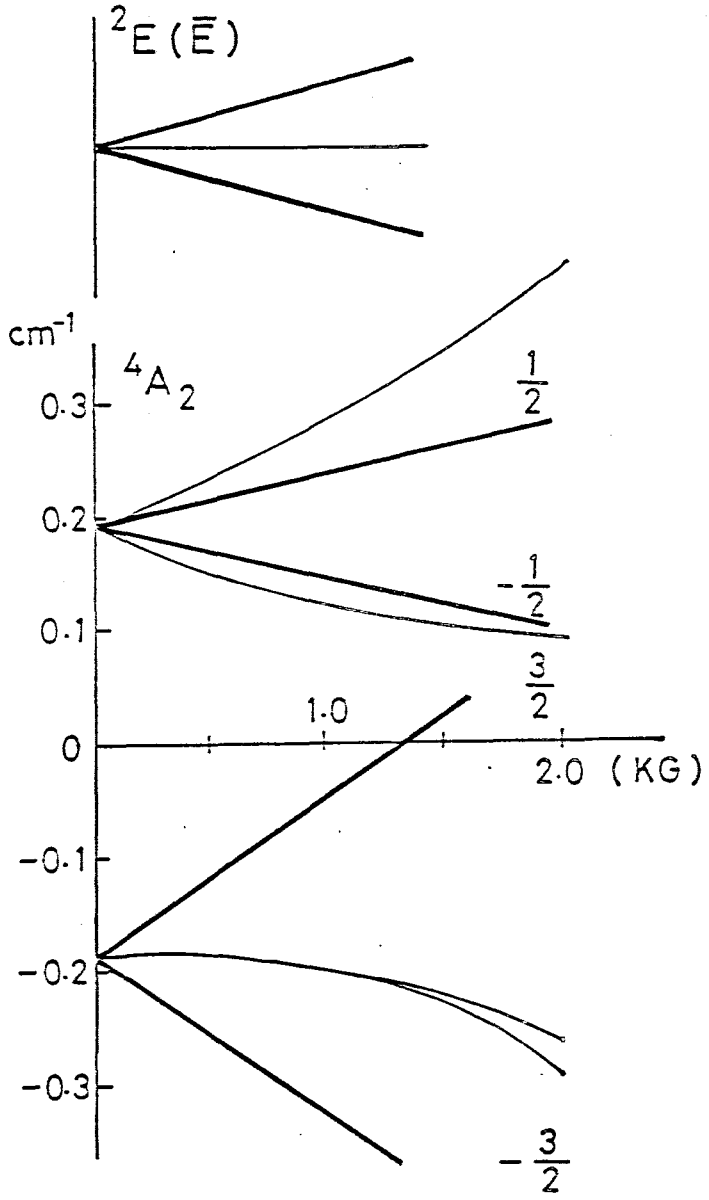

Fig. 5-(b)

Zeeman level splitting of the $^4A_2$ ground state and the first excited state $^2E(\bar{E})$ in ruby at $\theta = 0°$ and at $\theta = 90°$. The angle θ is taken between the magnetic field and the c axis of crystal. The heavy lines are at $\theta = 0°$ and the thin lines are at $\theta = 90°$. The level $^2E(\bar{E})$ is almost degenerate at $\theta = 90°$. The half-integer numbers attached to the heavy lines denote the spin magnetic number m of each level.

Table 1

Spin-lattice relaxation times on ruby obtained by the PM and the SQUID-ESR measurements. The angle θ is taken between the magnetic field and the c axis of crystal. The ESR transitions occur between levels m=± 1/2 at 440 G and between levels m=± 3/2 at 167 G. The Zeeman level splitting is shown in Fig. 5-(b).

Sample	0.01 %		0.05 %		0.3 %
angle	θ = 0°	θ = 90°	θ = 0°	θ = 90°	θ = 0°
PM 4.2 K 300 G			0.23 s	0.20 s	0.23 s
			0.65 s	------	------
PM 1.7 K 300 G	0.50 s	0.50 s	0.49 s	0.42 s	0.60 s
	1.95 s	------	1.35 s	------	------
ESR 4.2 K 440 G	0.16 s		0.40 s		
	0.72 s		------		
ESR 4.2 K 167 G	------		0.40 s		
	0.80 s		------		

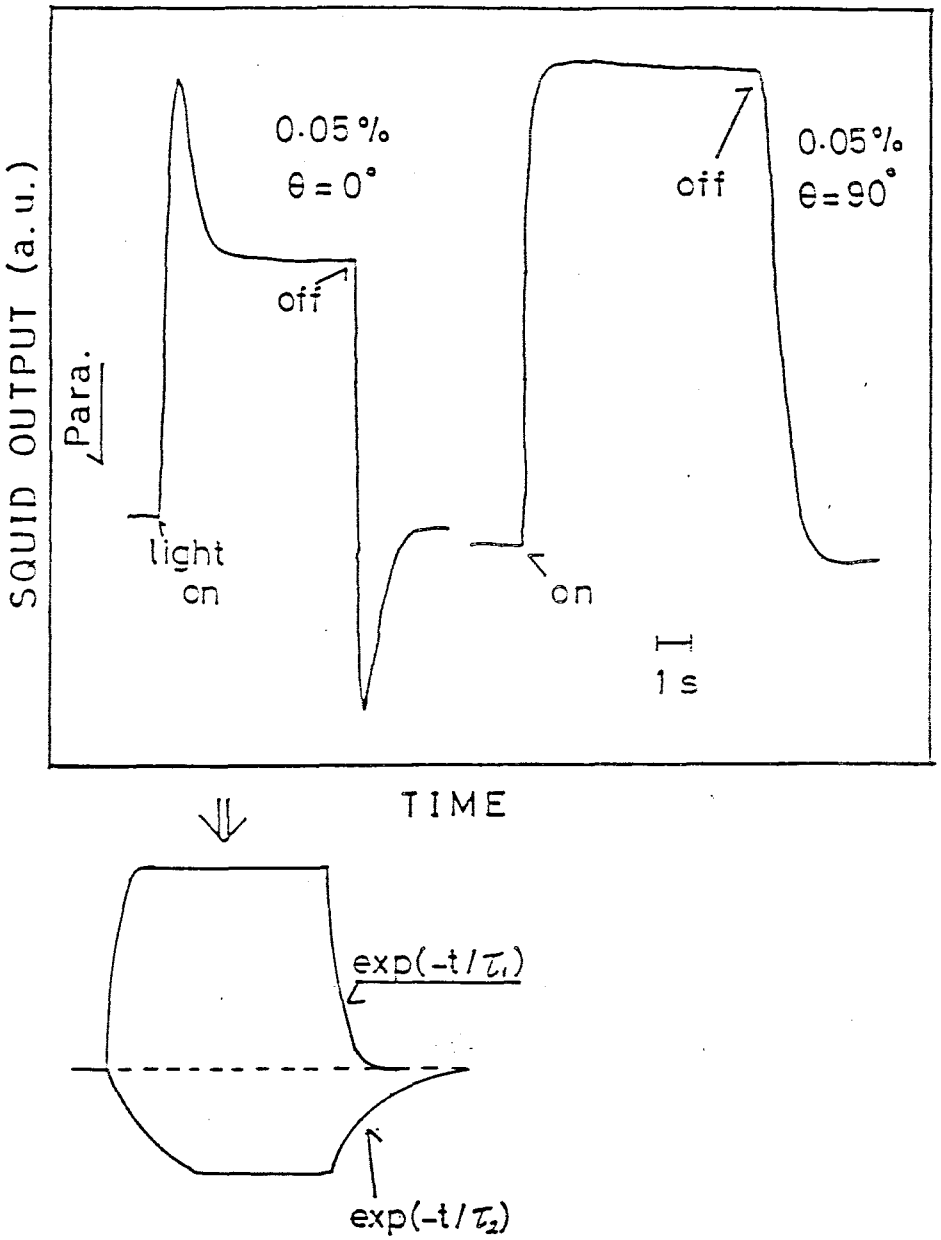

Fig. 6

The waveform of the PM signal measured on ruby with 0.05 mol% Cr^{3+} at 4.2 K at θ =0° and θ =90° . At θ =0° the signal is resolved into two components which are schematically shown in the lower side of the figure, while at θ =90° the signal consists of a single component.

2. Instruments for SQUID ESR Measurements

The SQUID detection of ESR (SQUID-ESR) measures decrease in longitudinal magnetization induced by ESR saturation, while the conventional ESR measures rf absorption proportional to the transverse magnetization. It has been shown[23] that the SQUID-ESR is superior to the conventional ESR in a low rf frequency region and for samples with a long spin-lattice relaxation time. Especially the SQUID gives a simple and direct method for observing the spin lattice relaxation process. Since the SQUID system needs extremely stable magnetic field(See Sec.II -1), rf frequency must be swept through resonance. In the previous work [20-23] the rf field was produced by a saddle coil. The saddle coil method should have a high frequency limit because the impedence of the coil will be much higher than that of the microwave oscillator and correspondingly the rf field on the sample is decreased with increasing the frequency. In this work the SQUID-ESR has been developed in the frequency region above 1 GHz which is higher than in the previous report.[23] For this purpose a coaxial cavity with a tunable resonance frequency has been introduced instead of a saddle coil. The coaxial cavity with a high Q-factor produces much intense rf magnetic field, which will enable us to apply the SQUID ESR to the samples with shorter spin lattice relaxation times than those in the previous work.

2-1. Theoretical Background

In the SQUID detection of ESR the decrease in the z component of M, Δ Mz, is measured by the SQUID magnetometer. In the steady state Δ Mz is obtained from the Bloch equations as follows[26]:

$$\Delta Mz = \chi_o H_o \frac{\eta}{1 + (\omega_o - \omega)^2 T_2^2 + \eta} , \qquad (2)$$

where the saturation factor $\eta = \gamma^2 H_1^2 T_1 T_2$, χ_o is the static susceptibility, γ the gyromagnetic ratio, H_o the static field, H_1 rf the magnetic field, ω the applied rf frequency, ω_o the resonance frequency of the sample, T_1 the longitudinal spin relaxation time, and T_2 the transverse one. In Eq.(2) we take the positive sign for the reduction of the spin polarization.

When the rf field is switched on and off the time dependent change, Δ Mz(t), is usually described as

$$\Delta Mz(t) = \Delta Mz \left[1 - \exp(-t/T_1^*) \right] , \qquad (3)$$

after the rf field is switched on, and

$$\Delta Mz(t) = \Delta Mz \left[1 - \exp(-t/T_1) \right] , \qquad (4)$$

after switched off, where Δ Mz is given in Eq.(2) and

$$T_1^* = \frac{T_1}{1 + \eta} . \qquad (5)$$

In the ESR spectrum measurement the saturation factor, η, must satisfy that $\eta \ll 1$ to prevent from the saturational broadening. Equation (2) predicts the lineshape to be a Lorentzian curve for the sample with homogeneous broadening.

At the center of the resonance frequency, $\omega = \omega_0$, ΔMz is proportional to H_1^2 when $\eta \ll 1$ and approaches to the complete saturation value $\chi_0 H_0$ when $\eta \gg 1$.

The observation of the spin relaxation process is made around the center of the resonance, $\omega = \omega_0$. The waveform of $\Delta Mz(t)$ described by Eqs.(3) and (4) is recorded. Accordingly the spin lattice relaxation time T_1 is obtained directly and the form of the relaxation curve is also analyzed. The maximum rf field intensity is necessary to be as large as possible to obtain a good signal to noise ratio and to apply the method extensively. If the rf field is supplied by the saddle coil, the impedence of the rf coil will be much higher than the oscillator output impedence ($\sim 50\ \Omega$), and correspondingly the rf field on the sample will be decreased with increasing rf frequency. Therefore in the GHz region the coaxial cavity is more suitable to supply the intense rf field than the saddle coil.

2-2. Experimental Arrangement

The SQUID-ESR measurement is different from the PM measurement only in use of microwave instead of light as an excitation. Figure 7 shows a block diagram of the measuring system used here. The cavity is placed inside the pick-up coils and the sample is mounted in the cavity. The sample position is at one of the pick-up coils. The magnetic field is fixed at about 400 G. Microwave with a frequency around 1 GHz is supplied by a Wavetek 2001 sweep oscillator. The oscillator must be tuned to the cavity. First, the amplitude of reflected wave from the cavity is observed through the bidirectional coupler and shows a sharp minimum at the cavity resonance, to which the oscillator frequency is tuned by automatic frequency control electronics. Second, the oscillator is operated in CW mode at the fixed frequency of the cavity resonance. Finally the microwave is modulated in amplitude for observing Δ Mz using a Hewlett-Packard HP-33000D modulator.

The modulation is carried out in two modes: square wave modulation; and pulse modulation. In the square wave modulation, the SQUID output is fed to a lock-in amplifier which is not shown in Fig. 7, and the modulation frequency must be smaller than T_1^{-1}. This mode is useful for samples with relatively short T_1, because the narrow bandwidth of the phase sensitive detection will improve the sensitivity of the system remarkably.

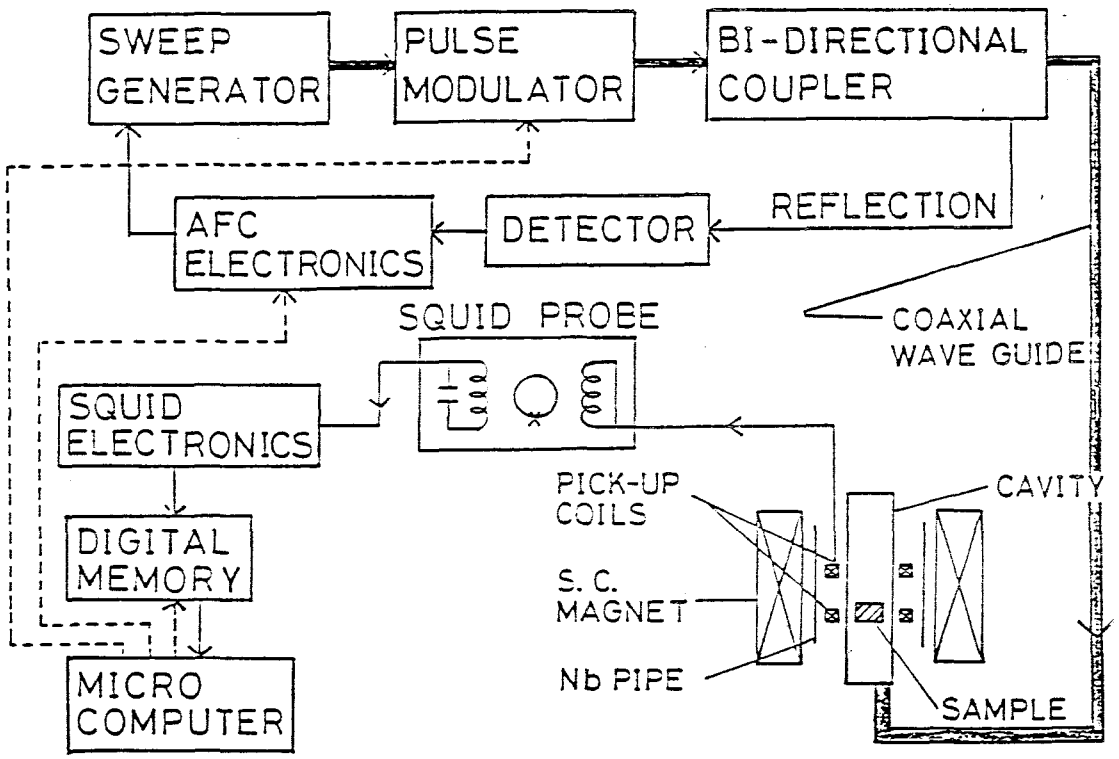

Fig. 7

Block diagram of the experimental arrangement for the SQUID-ESR measurement. The heavy lines indicate the transmission line of the microwave. The thin lines indicate the stream of the observed signal. The dashed lines indicate the control bus from the microcomputer.

In the pulse modulation the temporal change Δ Mz(t) is measured using the digital transient memory and is analyzed to obtain the amplitude Δ Mz and the relaxation time T_1. This mode is used for samples with too long T_1 to use the first mode. In addition the signal to noise ratio can be improved by averaging the waveform of Δ Mz(t) over a lot of pulses.

In the measurement of ESR spectrum either of the modes is chosen according to the value of T_1 of the sample. In our method the frequency is swept discretely and Δ Mz is measured point by point at each frequency. From the starting frequency the cavity frequency is changed successively by a certain frequency interval and the tuning process mentioned above is repeated. As a result the frequency dependence of Δ Mz gives the resonance line. In the measurements of the temporal change, only the second mode is used and the frequency is fixed at the center of resonance of the sample.

Figure 8 shows the coaxial cavity which is composed of an inner conductor of copper wire with 1 mm o.d. and an outer conductor of alminium pipe with 7 mm i.d.. The cavity is shortened at one end and is open at another. Since the outer conductor is slightly longer than the inner conductor, the cut-off behavior of the cylinder prevents from the radiation loss at the open end. The cavity frequency is changed by inserting a quartz plunger from the open end. The quartz plunger can be used also as a light guide in the experiment of photo-excitation.(See ChapterIV) The cavity length is chosen $5\lambda/4$ where λ is wavelength in free space and is about 25 cm.

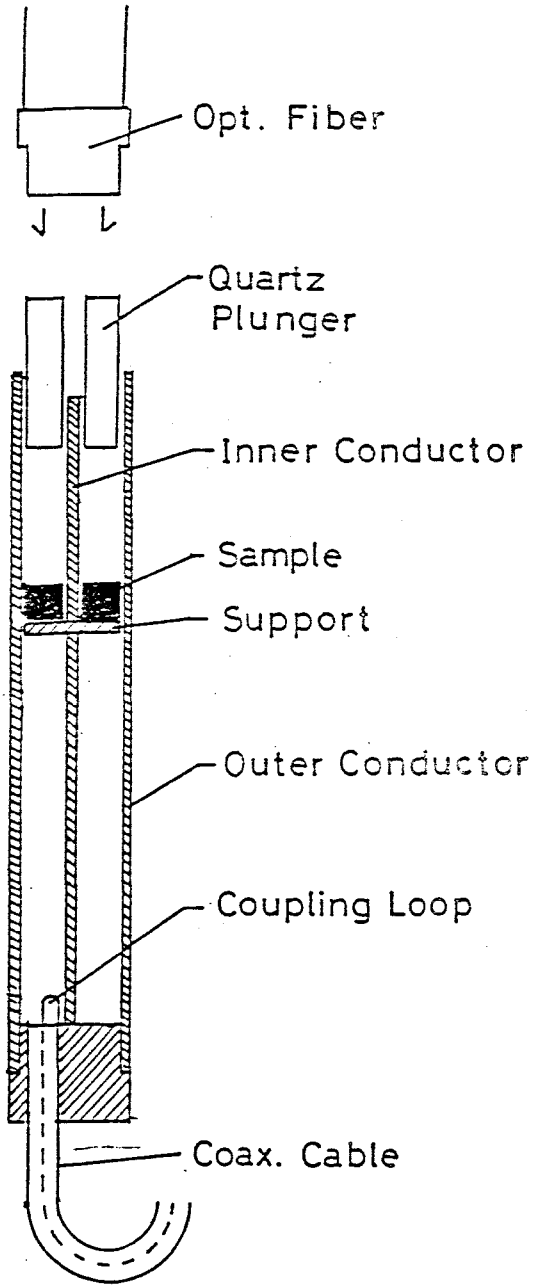

Fig. 8

Coaxial cavity used in the SQUID-ESR measurement near 1 GHz. The cavity frequency is varied by translating the quartz plunger, which is also used as a light guide. The sample support is made of teflon.

The Q-factor of the cavity is about 1600 at 4.2 K, and the tuning range of the frequency is about 100 MHz with a plunger of 40 mm in length. Use of the dielectric plunger is more convenient than the usual metal plunger because the former is completely free from the electric contact between the plunger and the both inner and outer conductors. The rf field is fed to the cavity through H-coupling at the shortened end. The coupling between the cavity and the transmission line (50 Ω) is made critical by adjusting the size and the angle of the H-coupling loop. The sample is placed at the maximum position of the rf magnetic field H_1, and the static field H_o is applied along the cavity axis. The magnitude of H_1 at the sample position is estimated about 10^{-1} G when the output power of the oscillator is 10 mW, and the variation of H_1 is estimated at 5% throughout the measuring frequency range. The magnitude of H_1 must be as constant as possible because the change in magnetization is proportional to H_1^2 and the variation of H_1 produces a spurious structure in the ESR spectrum.

2-3. Demonstration of SQUID-ESR

(1) DPPH

DPPH(1,1-Diphenyl1-2-picrylhydrazyl) is usually used as a standard sample in the ESR experiment. It is known that the g value is 2.0036 and the resonance line is exchange-narrowed. We used the resonance frequency for calibrating the static field H_o at a sample. The observed resonance line shown in Fig.9-(a) fits well to a Lorentzian curve denoted by the solid line. The FWHM (Full Width of Half Maximum) is 17.5 MHz which corresponds to 6.25 G. Figure 9-(b) shows the wave form Δ Mz(t) at the center of the resonance. The rise and decay forms are described by Eqs.(3) and (4). The rise time is 1470 ms and the decay time is 640 msec, which is not consistent with Eq.(5). The steady state amplitude during saturation is proportional to the rf power up to the maximum power of 10 dbm. This result indicates that the saturation factor η is small enough compared to unity.

The spin lattice relaxation in the exchange-interacting system, e.g. DPPH, was studied previously by Goldsborough et.al.[27], and has not been completely understood especially at low temperature. Here we present only the observed result, but do not enter the physics of spin-lattice relaxation in DPPH.

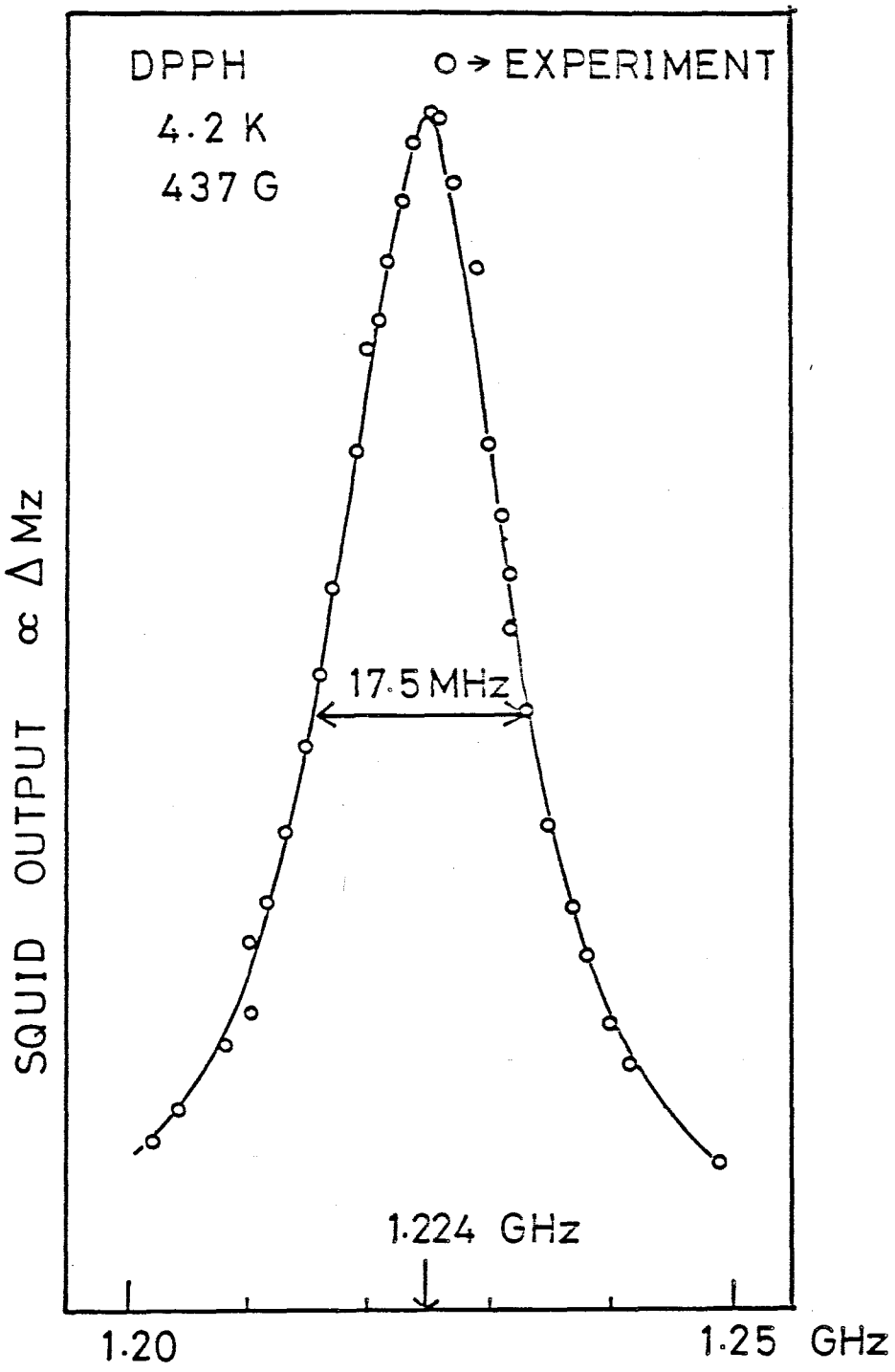

Fig. 9-(a)

ESR lineshape of undiluted DPPH powder at 4.2 K. The points are experimental and the solid line denotes a Lorentzian curve with the best fit. The FWHM is 17.5 MHz, which corresponds to 6.25 G.

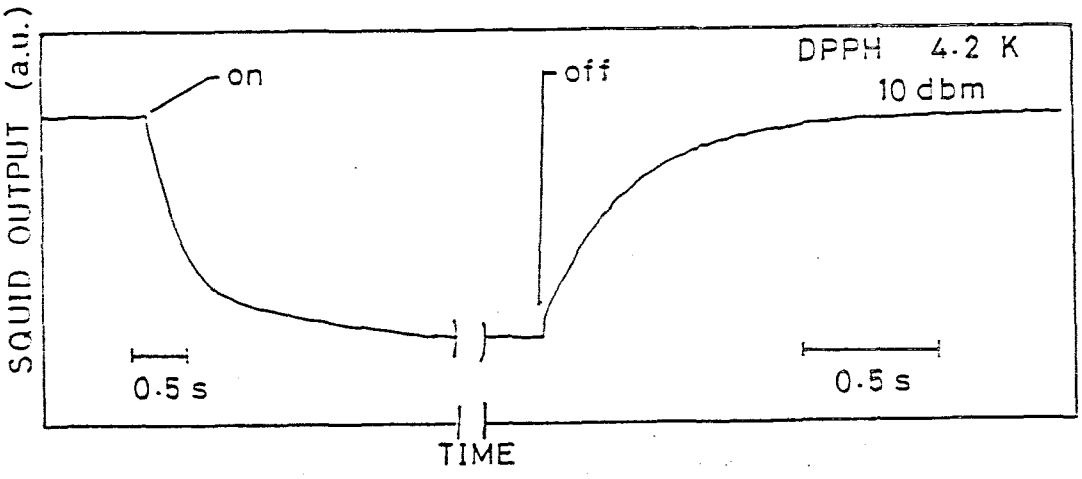

Fig. 9-(b)

Waveform of Δ Mz(t) on DPPH observed for a microwave pulse at the ESR line center at 4.2 K. The time scale is different between the rise part and the decay part as indicated in the figure.

(2) RUBY

The samples used here were ruby with 0.01 mol% Cr^{3+} and with 0.05 % Cr^{3+}. The static field H_o was applied parallel to the c-axis, namely, $\theta = 0°$. The ESR saturation occurs between levels $m = \pm 1/2$. On 0.01 % sample, a typical trace of the temporal magnetization change for an rf pulse is shown in Fig.10 at 4.2 K and at 440 G. This signal is similar to the PM signal shown in Fig.6. The signal consists of two different components. One is diamagnetic and its relaxation time after the saturation is 0.16 sec. Another is paramagnetic and the relaxation time is 0.74 sec. Only the diamagnetic component is induced by an rf pulse whose width is short enough compared to the longer relaxation time. In this case, the rf power is reduced to prevent from the saturational broadening, and the lineshape of Δ Mz is shown in Fig. 11. The line shape is a Gaussian curve with the FWHM of 57 MHz,i.e., 20 G.

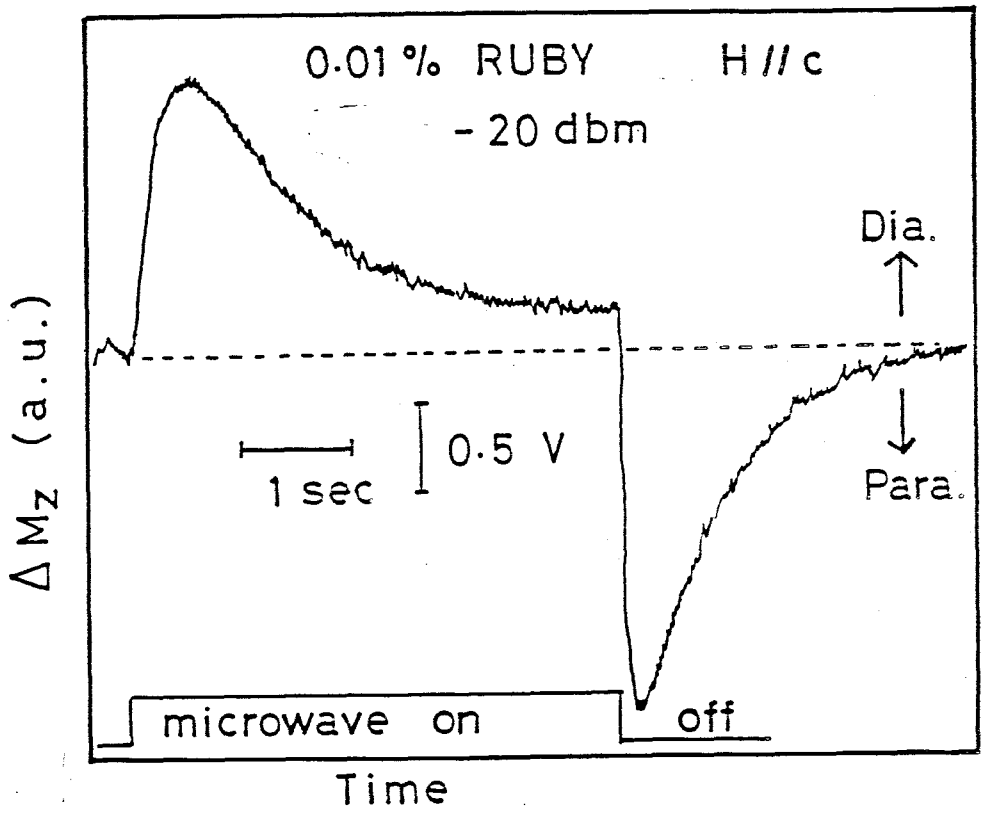

Fig.10

Temporal waveform of Δ Mz(t) measured on 0.01 % ruby in H // c at 4.2 K when a long saturating microwave pulse is applied. The ESR transition occurs between levels m=± 1/2. The waveform is resolved into two components as similar in Fig. 6.

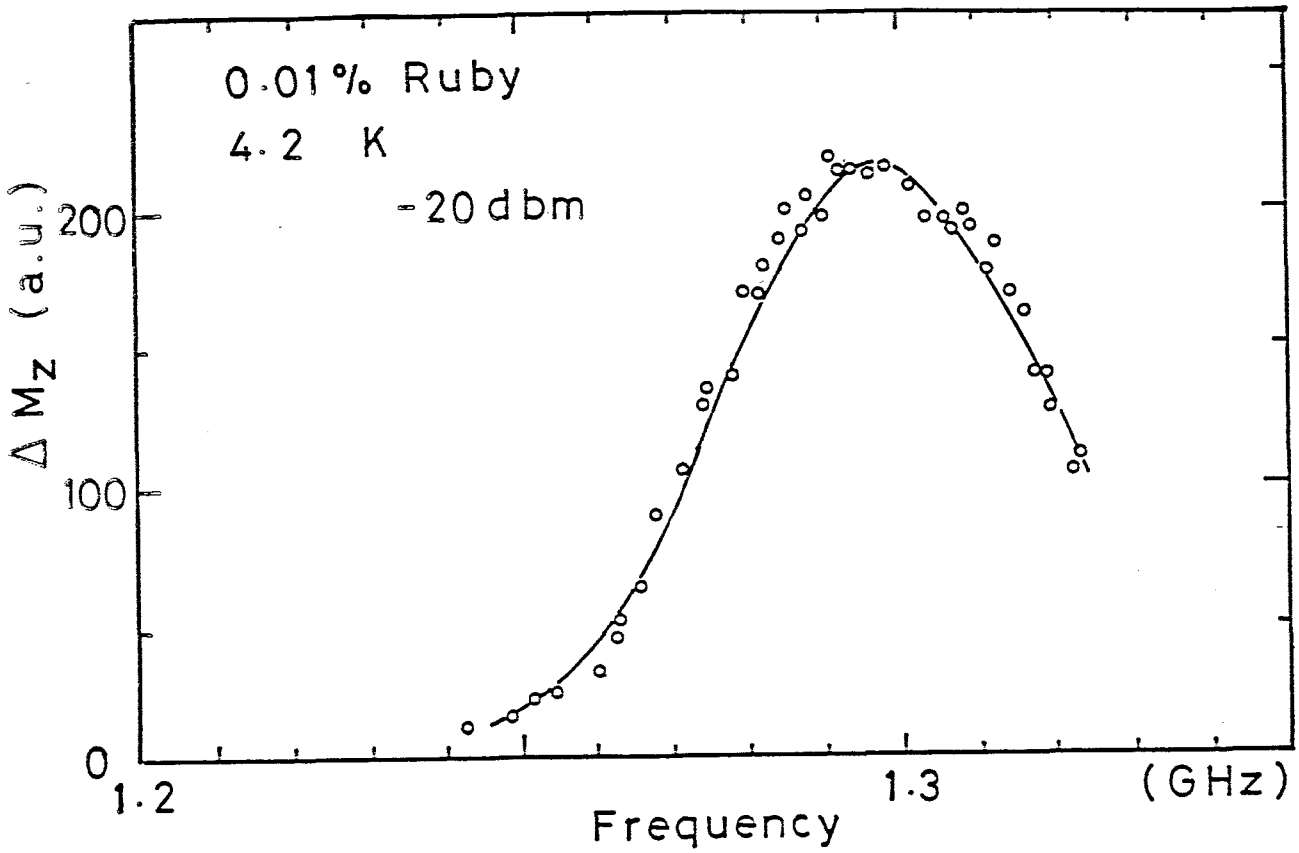

Fig.11

ESR lineshape for transition between levels of $m=\pm 1/2$ observed under the unsaturated condition. The points are experimental and the solid line denotes a Gaussian curve with the best fit. The FWHM is 57 MHz which corresponds to 20 G.

For the sample with 0.01 mol% Cr^{3+} ions, another experiment was made. The ESR saturation between levels m=± 3/2 is induced at about 150 G at θ =0° , i.e. one third of the magnetic field for transition between levels m=± 1/2. Though the resonance line is too broad to find the peak, the relaxation time after the saturation is 0.80 sec at 4.2 K. This result indicates that the longer relaxation time mentioned above is associated with levels m=± 3/2. Since the transition of Δ m=± 3 is forbidden in the ESR, the reason why this transition is observed remains in question.

On the more doped sample with 0.05 mol% Cr^{3+} ions, the feature is quite different from that of 0.01 % ruby, and also different from the PM signal shown in Fig. 6. The signal consists of a single diamagnetic component only. The relaxation time after the saturation is 0.4 sec at 440 G and at 4.2 K. This relaxation time is an intermediate value between the shorter and the longer T_1 of the 0.01% ruby. The resonance line is almost the same as that of the 0.01 % ruby.

3. Discussion and Conclusion

We will discuss the origin of the PM effect and the spin lattice relaxation process in ruby in this section.

On 0.01% ruby sample at $\theta = 0°$, the waveform of the PM signal and its relaxation time are almost the same as that of the SQUID-ESR . Therefore we conclude that the photoexcitation produces a population change from thermal equilibrium in the Zeeman levels of the ground state $^4A_2$ like the ESR. Accordingly the decay of the PM signal is due to the spin-lattice relaxation. As shown in Fig. 5-(a), the excitation light of Hg lamp induces the optical transition from the ground state to the excited states $^4F_1$ and $^4F_2$, which are relaxed to the lowest excited state $^2E(\bar{E})$ by the nonradiative process in very short time. The state $^2E(\bar{E})$ has a relatively long lifetime of the order of 10^{-3} sec. The transition from the state $^2E(\bar{E})$ to the ground state occurs radiatively with a high quantum efficiency. In the presence of the static magnetic field at $\theta = 0°$, the optical transitions occur according to relative transition rates indicated by the numbers[28] as illustrated in Fig. 5-(a). As a consequence the spin polarization of the ground state is changed from thermal equilibrium by the photo-excitation.

Next we discuss the spin-lattice relaxation in the ground state for 0.01 % ruby. The two decay components are observed in both the PM and ESR measurements. We use the same symbols τ_1 and τ_2 for the shorter and the longer relaxation time, respectively. It is generally expected that two components appears in the spin-lattice relaxation in a multi-level spin system

with $S \geqq 1$, if the transition probabilities between different pairs of states are different. In the case that H // c, the spin Hamiltonian yields the diagonal matrix elements only and the Zeeman levels are described well by the spin magnetic quantum number, m. The change in magnetization Δ Mz is expressed as

$$\Delta Mz/\beta = (\Delta n_{1/2} - \Delta n_{-1/2}) + (\Delta n_{3/2} - \Delta n_{-3/2}), \qquad (6)$$

where Δn_m denotes change in population of level m from each thermal equilibrium value and β the Bohr magneton.
The quantities Δn_m satisfy the conservation of the total ion number, $\Sigma_m \Delta n_m = 0$. Here we assume g = 2 for simplicity and use the positive sign of Δ Mz to be diamagnetic. On the other hand, since the ground state is non-Kramers state, the spin-lattice interaction is given by a quadratic form of spin operators[29] and consequently the selection rule for the spin lattice relaxation is given as $\Delta m = \pm 1$ and ± 2. In Fig. 5-(b), among six relaxation transitions in the ground state, one transition between levels $m = \pm 3/2$ is forbidden and others are allowed.

The shorter relaxation time τ_1 is assigned to be the spin-lattice relaxation time between levels $m = \pm 1/2$, since its value agrees with the previous result[30] obtained from the decay of the rf absorption after the ESR saturation in the conventional method. On the other hand the longer relaxation time τ_2 is associated with the population change of the levels $m = \pm 3/2$. The direct transition between levels $m = \pm 3/2$ is forbidden because $\Delta m = 3$, and therefore the relaxation takes place via transitions to other two levels $m = \pm 1/2$.

When a short microwave pulse is applied, only the first term in the right hand of the Eq.(6) is changed toward the diamagnetic,i.e., positive direction, while the second term remains unchanged owing to the long relaxation time. Consequently only the faster diamagnetic component is observed for the ESR saturation with a short rf pulse.

Next, when the pulse width is so long that the relaxation from levels $m=\pm 1/2$ to $m=\pm 3/2$ occurs, the last term of Eq.(6) contributes to Δ Mz. Observation shows that this contribution is paramagnetic, i.e.$(\Delta n_{3/2} - \Delta n_{-3/2}) < 0$, which is attributed to that the relaxation rates with $\Delta m=2$, i.e., +1/2 to -3/2 and +3/2 to -1/2 are larger than those with $\Delta m=1$, i.e., +1/2 to +3/2 and -3/2 to -1/2. Accordingly τ_2 is assigned to a time in which the population of levels $m=\pm 3/2$ returns to thermal equilibrium through the relaxation to levels $m=\pm 1/2$.

The similar relaxation process occurs in the PM effect in ruby. The disappearance of the slower relaxation process in 0.3 % ruby may be due to an increase of the cross relaxation rate, which depends on the concentration of the paramagnetic impurities.

On the 0.05 % ruby at $\theta = 0°$, the PM measurement gives the same feature as for the 0.01 % ruby, while the SQUID-ESR measurement gives quite different result as illustrated in Table 1. The reason of this different has not been resolved yet.

From the above discussion we conclude that the SQUID detection of the PM effect and the ESR is more useful and more convenient for studying the spin-lattice relaxation than the conventional method. This advantage arises from the fact that the SQUID

method can measure a non-equilibrium change in magnetization totally. Namely, the conventional ESR method gives mainly the information associated with the states in resonance, while the SQUID method gives another information associated with non-resonant states.

In conclusion the experimental system for the PM and the ESR measurement using a SQUID magnetometer has been constructed. In the SQUID-ESR measurements, a tunable coaxial cavity is employed successfully in the GHz region, and the advantage for observing the spin relaxation is demonstrated. In both measurements the spin-lattice relaxation in ruby is demonstrated as a test of the system. However the phenomena observed include unresolved problems, and therefore these phenomena will be studied in the future work in detail. In addition the PM effect and the ESR are considered to be in complementary relation with each other.

ChapterⅢ PM Effect on Shallow Donors in Si

1. Experimental Arrangement

The experimental arrangement is essentially the same as described in the ChapterⅡ .1, and the only difference is shown in Fig. 12.

The excitation light is extrinsic IR light, namely, $h\nu < E_g$, where E_g is the Si energy gap of 1.15 eV. One of light sources is a tungsten lamp with a short wavelength cut-off filter of Ge which is used for the purpose of removing the intrinsic light ($h\nu > E_g$). The cutoff wavelength of Ge is about 1.8 μm. Another source is a CO_2 laser with a wavelength around 10 μm. The exciting light is gated by a mechanical shutter and is guided to a sample through a Cu-Ni light pipe. The quartz light guide above the sample shown in Fig. 4 was removed.

Since the room temperature background (RTBG) radiation inevitably reaches the sample and has considerable affects on the PM effect (See ChapterⅢ .2), the RTBG intensity is diminished by cold filters placed in liquid helium. The transmission characteristics of the filters are illustrated in Table 2. When the CO_2 laser is used, the laser line almost coincides with the peak of the RTBG radiation in wavelength, and accordingly the RTBG radiation cannot be entirely removed.

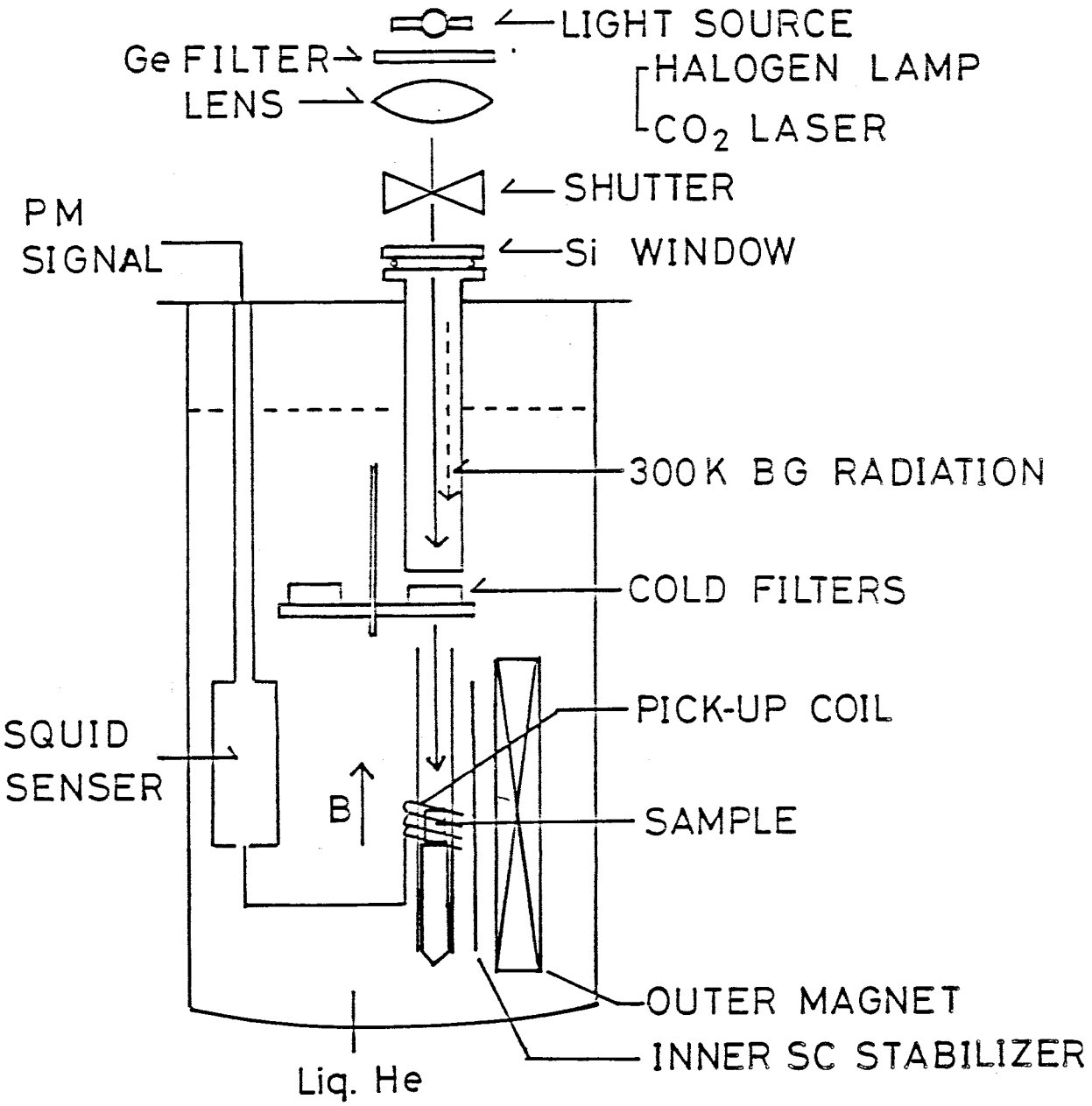

Fig.12

Experimental arrangement for measuring the PM effect on the shallow donors in Si. The RTBG radiation is attenuated variously by cold filters which are changeable by rotating the turn table.

Table 2

Transmission characteristics of the filters: The transparent region in wavelength and the relative BG intensity g_o. Transmission wavelength indicates the range for the transmittance above about 50%. The shorter wavelength is limited by the Ge filter and the longer one depends on each filter.

FILTER	TRANSMISSION WAVELENGTH (μ m)	RELATIVE BG INTENSITY
GLASS	1.8 ~ 3	0.2
Al_2O_3	1.8 ~ 5	3.1
MgO	1.8 ~ 10	16.5
NaCl	1.8 ~ 18	16.5< <192
NO FILTER	1.8 ~ ∞	192

The relative values of exciting light intensity g_{ex} and the RTBG intensity g_o are measured from the photoconductivity using a sample prepared from the same ingot as used in the PM measurements. Therefore, g_{ex} and g_o denote the experimental quantity proportional to photo- excited carrier concentration on the assumption of a constant mobility. The experimental detail will be described in ChapterV .1. In the tungsten lamp excitation, g_{ex} is controlled by the voltage across the lamp. The relation of the lamp voltage to g_{ex} is listed in Table 3.

The sample is immersed into liquid helium to prevent from heating induced by photo-irradiation as described in Sec.II -1. The sample volume is 3x3x5 mm^3. The sample is polished using first #2000 carborandom, next using 1 μm almina polishing powder, and finally is chemically etched using a solution of HNO_3 : HF : HCOOH = 5 : 3 : 1. Samples used are n-type and p-type Si in the low concentration region. In below we use the following abbreviation for indicating the sample : sample 9-16 P denotes Si doped with 9 x 10^{16} P/cm^3.

For sample 9-16 P, compensation effect on the PM effect was examined. The compensation was made by fast neutron irradiation at 300 K at Kyoto University Reactor Research Institute. Before the irradiation, the resistivity of the sample was about 0.1 Ω cm, and after the irradiation and the annealing at 200 ℃, it changed to 0.2 Ω cm. This result indicates that the degree of compensation is 50 % . The compensation centers are probably deep acceptor states associated with vacancies, e.g., neutral divacancies,[32] V_2^o. As a consequence, almost all of acceptors V_2^o are converted to the negatively charged state V_2^-, while half

of neutral donors D^O are ionized to D^+. We use the abbreviation 9-16 P(C) after compensation of sample 9-16 P in below.

The samples used in the present study are 2.2-16 P, 9-16 P, 9-16 P(C), 1.5-17 P, 3-17 P, 1-17 Sb, and 6-16 B. Sample 6-16 B is only p-type and the others are n-type.

Table 3

The relative value of excitation intensity g_{ex} versus the applied voltage of a tungsten lamp. The value of g_{ex} is determined by the photoconductivity, and is proportional to the photoexcited carrier concentration. The cold filter used is Al_2O_3 filter.

LAMP VOLTAGE (V)	RELATIVE EXCITATION INTENSITY g_{ex}
2.5	1.9
5.0	4.9
7.5	7.8
10.0	10.0
12.5	12.5
15.0	14.8
17.5	15.4
20.0	16.9

2. Experimental Results

2-1. Characteristic Features of PM Effect

A typical trace of the PM signal is shown in Fig. 13 for sample 9-16 P at 750 G and at 1.6 K. The excitation source was a tungsten lamp and a glass plate was used as a filter. When the photo-excitation is turned on, the magnetization varies towards the diamagnetic direction, and when turned off the magnetization returns to its thermal equilibrium value. The steady state amplitude during the excitation is denoted as A_{ex} which is proportional to the change in magnetization, and $\tau_{1/2}$ is a half decay time after the photo-excitation is turned off. Observation shows that the decay curve is not exponential. The semilogarithmic plot of the curve indicates that a faster decay component appears in the beginning part of the decay as shown in Fig . 21-(b).

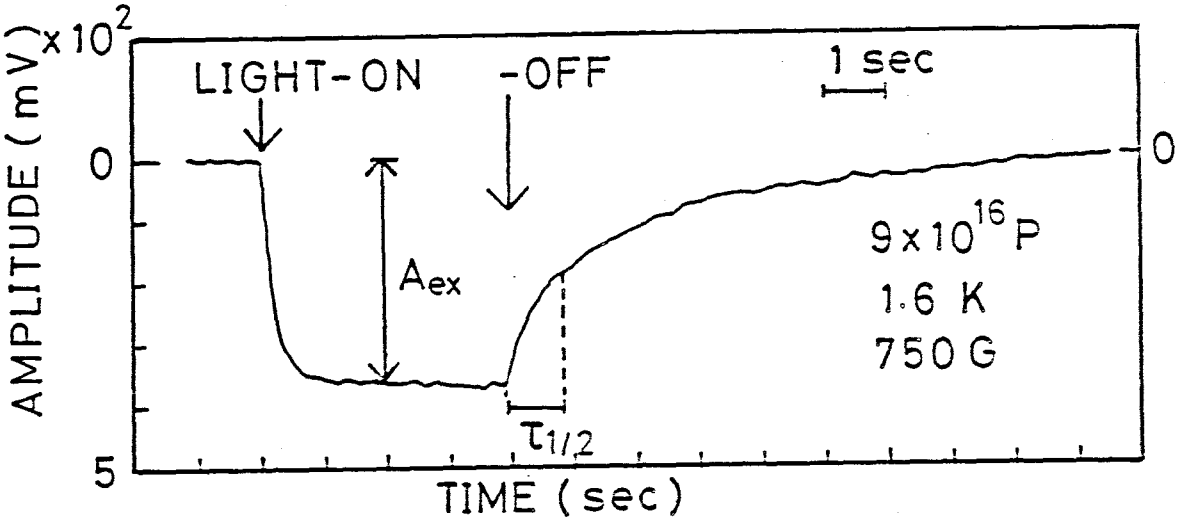

Fig.13

PM signal measured with combination of a tungsten lamp and a glass filter at 1.6 K and at 750 G. The quantities A_{ex} and $\tau_{1/2}$ are the steady state amplitude and the half-decay time, respectively.

The PM effect was observed for samples doped with other species of impurity. Sample 1-17 Sb gives essentially the same results as a phosphorus doped sample. On the p-type sample 6-16 B, however, the PM signal was not observed.

The compensation has a remarkable influence on the PM effect. Namely, as mentioned above, sample 9-16 P(C) contains 4.5×10^{16} P/cm^3, and therefore the PM signal amplitude is expected to be one half of the uncompensated sample, if the signal is proportional to the neutral donor concentration. Nevertheless, we observed no PM signal on sample 9-16 P(C).

The quantities A_{ex} and $\tau_{1/2}$ depend on the excitation intensity g_{ex}, the RTBG intensity g_o, the sample temperature T, and the donor concentration $N(D^o)$. These dependences will be discussed in detail in the following sections.

2-2 Half Decay Times

The dependences of the half decay time $\tau_{1/2}$ on the RTBG intensity g_o, the temperature T, and the donor concentration $N(D^o)$ are presented in this section.

The dependences of $\tau_{1/2}$ on T and g_o are shown in Fig. 14 for sample 9-16 P at 750 G. The RTBG light intensity g_o is attenuated to various degree by choice of cold filters as shown in **Table 2.** With increasing g_o, $\tau_{1/2}$ decreases and becomes independent of temperature. Besides, the additional BG light is supplied on the sample using a tungsten lamp with a Ge filter, which is not shown in Fig. 12. The intensity of the tungsten lamp background (TLBG) light is estimated in the same way as the excitation intensity g_{ex}. Since the TLBG light has a role on the generation of background photocarriers similar to the RTBG light. The observed relaxation rates, $\tau_{1/2}^{-1}$, are plotted against the TLBG intensity, g_o^*, in Fig. 15. The important conclusion is that the increase in the relaxation rate is proportional to the photo-excited carrier concentration. These features are also observed for sample 2.2-16 P.

The dependence of $\tau_{1/2}$ on the phosphorus concentration $N(D^o)$ is shown in **Fig. 16** . With increasing $N(D^o)$, $\tau_{1/2}$ monotonically decreases. Moreover, the reduction in $\tau_{1/2}$ induced by the BG radiation disappears above 1.5×10^{17} P/cm^3.

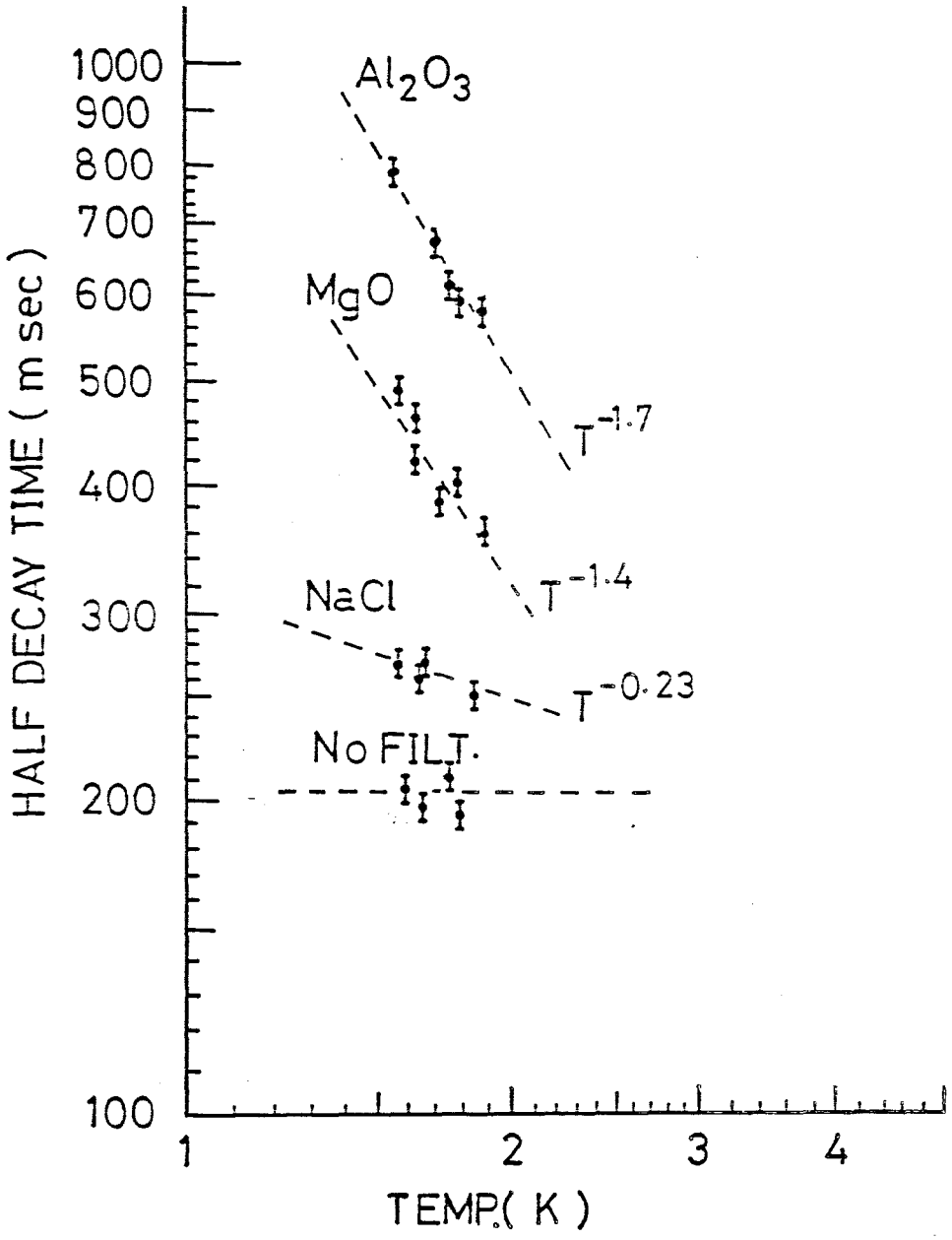

Fig.14

The temperature dependence of $\tau_{1/2}$ measured with different cold filters. The characteristics of the filters used are listed in Table 2. With increasing the BG intensity, the half decay time is decreased and the temperature dependence becomes weak.

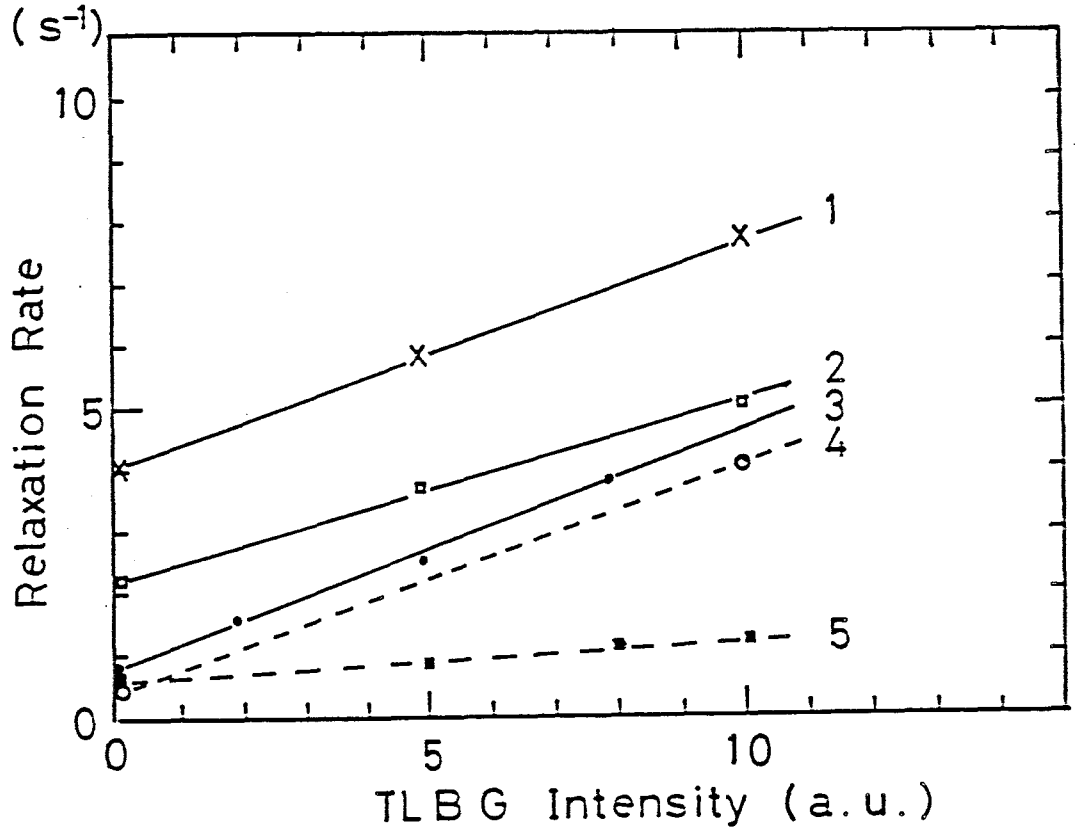

Fig. 15

The relation of the relaxation rate $\tau_{1/2}^{-1}$ versus the TLBG intensity obtained by PM and ESR measurements. The points are experimental and the lines are drawn according to Eq.(10). The integer numbers denote different experimental conditions. No 1 to 3 are of the PM measurement, and No4 and 5 of the SQUID-ESR. Sample 9-16 P is used for No 1 to 4, while sample 9-16 P(C) for No 5. The exciting condition is different as below: No 1 denotes CO_2 laser excitation with the NaCl filter at 1.7 K, No 2 CO_2 laser excitation with MgO filter at 1.7 K, No 3 tungsten lamp excitation with the glass filter at 1.9 K. No 4 and 5 are the ESR results with the quartz filter at 1.7 K.

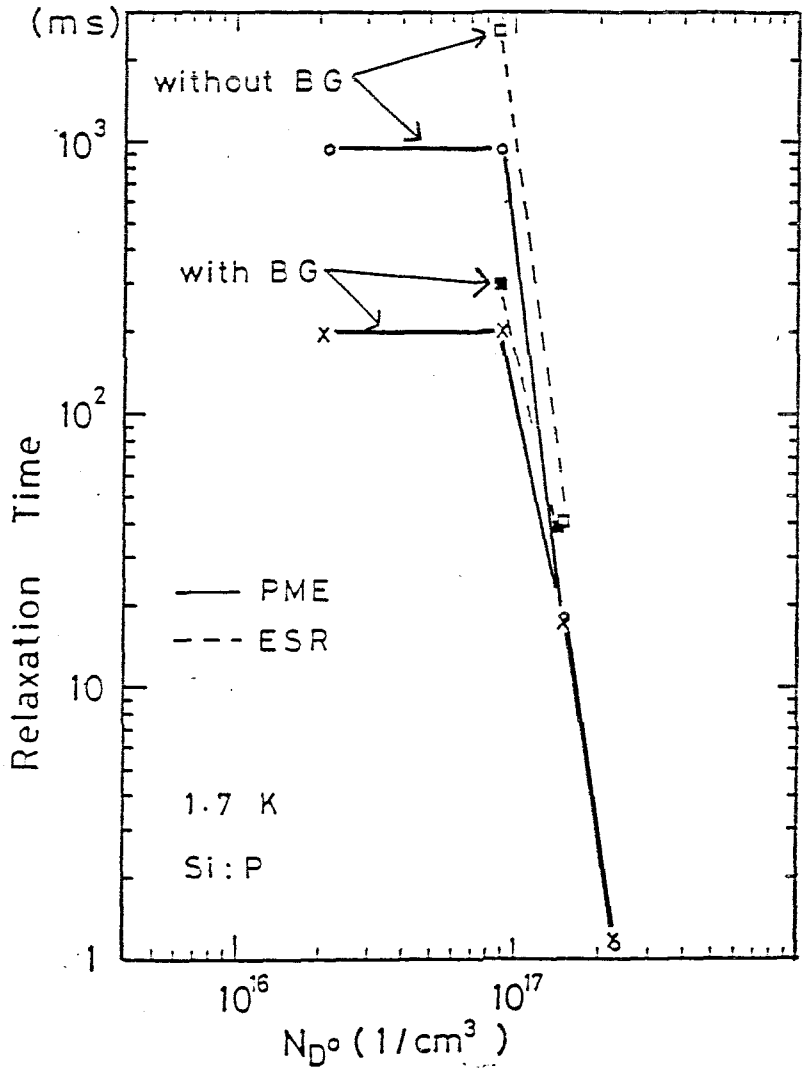

Fig. 16

Comparison of the relaxation times at 1.7 K measured by the PM effect and the SQUID-ESR for various donor concentration. The points are experimental and the lines are guide for eyes. The crosses and the open circles are obtained from the PM measurement at 750 G with and without the BG radiation, respectively. In the PM measurement the relaxation time is expressed by the half decay time $\tau_{1/2}$. Above concentration of 1.5 x 10^{17} P/cm^3 the relaxation times become independent of the BG radiation. The closed and open squares denote the SQUID-ESR measurement at 440G with and without the BG radiation, respectively. In the SQUID-ESR measurement the relaxation time is obtained from the slope of the semilogarithmic plot of the decay curve.

2-3. Amplitude of PM-Signal

In Fig. 17, the amplitude, A_{ex}, is plotted against the excitation intensity, g_{ex}, for the sample 9-16 P at 1.8 K and 750 G with and without the glass filter. Both results show a tendency of saturation in the amplitude A_{ex} with increasing the excitation intensity. The excitation source is the tungsten lamp. The RTBG light is almost removed when the glass filter is used. In the presence of the RTBG light, A_{ex} decreases as shown in Fig. 17.

The dependence of A_{ex} on phosphorus concentration shows a peak around 1×10^{17} P/cm^3 as illustrated in Fig. 18.

The amplitude A_{ex} also depends on the temperature, which is not shown. With decreasing temperature, A_{ex} is increased.

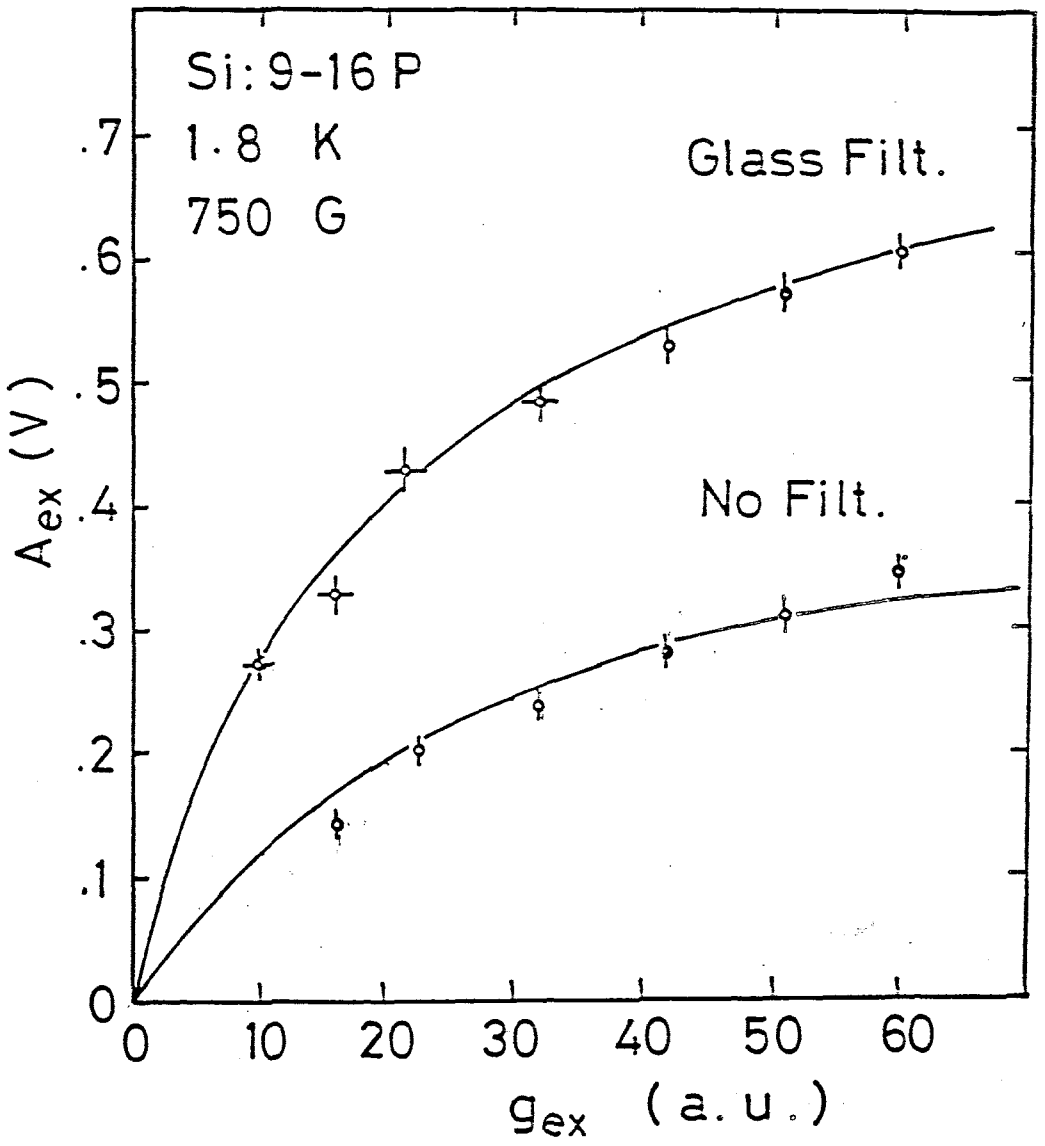

Fig. 17

The amplitude A_{ex} versus the exciting light intensity g_{ex} with and without the glass filter. The solid line is drawn according to Eq.(13).

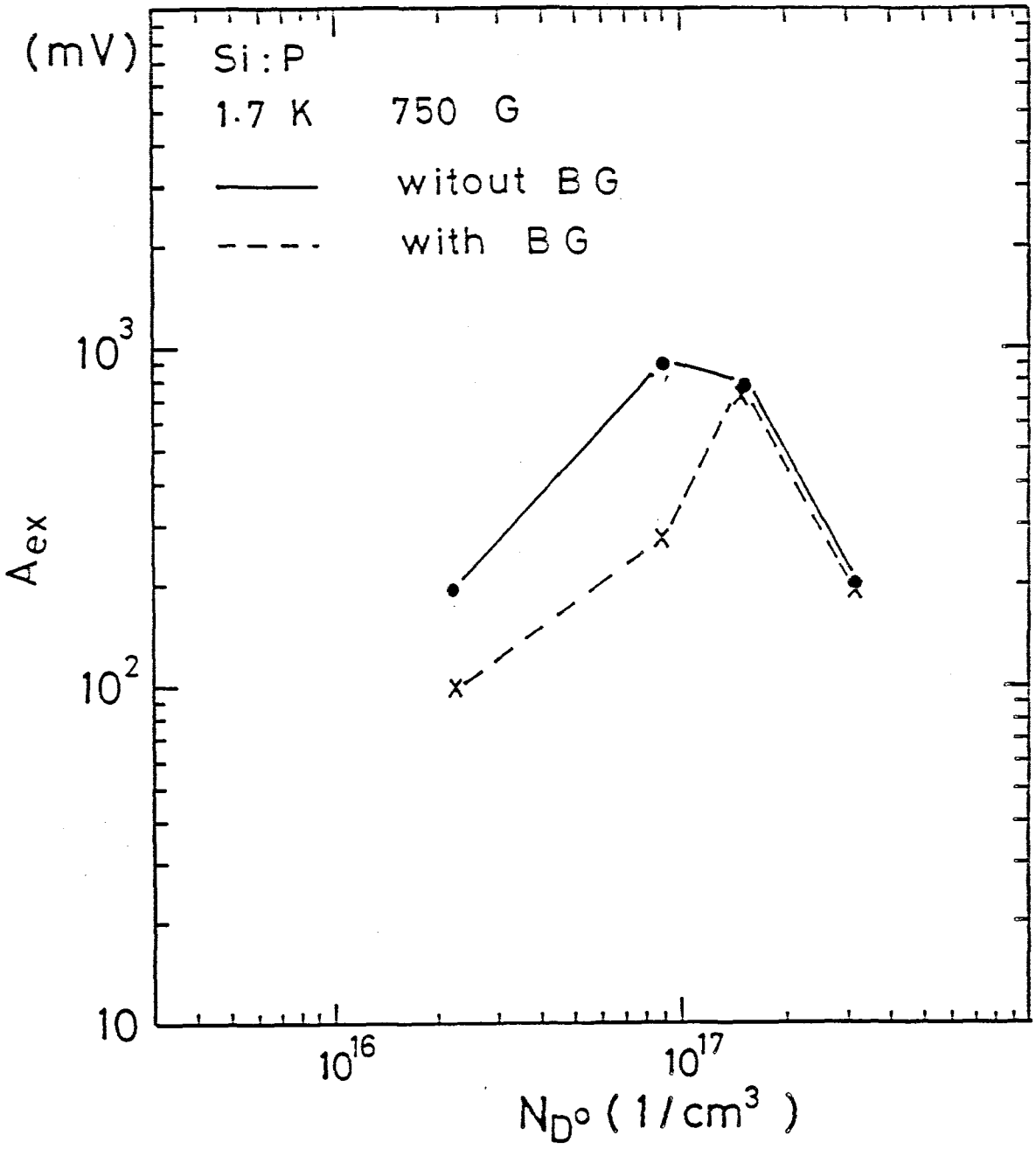

Fig. 18

Donor concentration dependence of the signal amplitude A_{ex} at 1.7 K and at 750 G under the same excitation intensity. The crosses and the closed circles are measured with and without the BG light, respectively. The lines are guide for eyes.

2-4. FIR Laser Excitation

As mentioned in Chapter I .1, when an IR light is illuminated on a sample doped with shallow impurities at a low temperature, the D^- states are produced. On the other hand, it is apparent that the FIR light destroys D^- states by photo-excitation of the excess electron of the D^- state. If the PM signal is ascribed to the diamagnetism due to the large electron orbit of a D^- state, we expect a decrease in the PM signal amplitude by the FIR illumination. The relation of the PM effect to the FIR light was examined on sample 9-16 P. As shown in **Fig. 19** the PM signal associated with FIR laser light was observed only in the presence of the IR light. The FIR laser lines used here were 170 and 393 μ m. No difference on the experimental results was observed between two wavelengths. When the FIR light was illuminated on superposition of the IR light, the observed signal amplitude is increased contrary to the above expectation, and the decay time of the signal is not affected by the FIR light. Accordingly this result cannot be simply understood in terms of the diamagnetism of the D^- states.

Concerning the amplitude of the PM signal, the ratio of the amplitude induced by the FIR light to that by the IR light only is about 1/4, while the ratio of the free carrier concentration induced by the FIR light to that induced by the IR light is of the order of hundredth. The change in diamagnetic moment is much larger compared with that of photo-carriers.

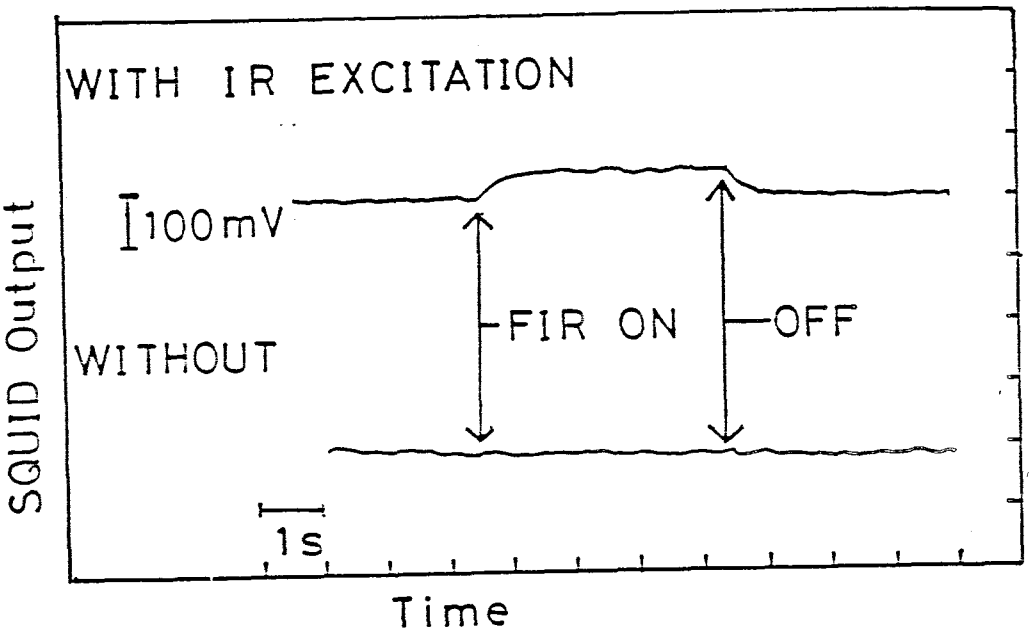

Fig. 19

The PM signal for the FIR light with and without IR excitation. The signal was observed only with IR excitation, and the FIR illumination increases the PM signal amplitude..

3. Discussion and Summary

We discuss the origin of the PM-effect in this section.

In general the photo-irradiation produces the inevitable rise in lattice temperature T_L which leads to the rise in spin temperature T_S. Accordingly the spin polarization of donors is decreased, which may be sensed by the SQUID system. If the observed signal is attributed to the rise in T_S due to a rise in T_L, the relative rise $\Delta T_L/T_L$ is estimated to be 23 % from the signal amplitude as explained below. This rise is considered too large and must not occur, because the sample is in good contact with the liquid He bath. Hence we conclude that the contribution of the rise in T_L is negligible.

Concerning other origin of the PM effect, we assume two possibilities as follows: i) the spin depolarization in the neutral donors; and ii) the orbital diamagnetism of the D^- states. For comparison with the experimental results, we rewrite Eq.(1) given in Chapter I as

$$\frac{\Delta Mz}{N(D^O)\beta} = \frac{\beta H_O}{kT_L}\,\frac{T_S - T_L}{T_S} + \frac{\beta H_O}{(m^*/m_O)^2\, E(D^-)}\,\frac{N(D^-)}{N(D^O)} \quad , \qquad (7)$$

where ΔMz is the decrease in magnetization observed. The maximum value of A_{ex} observed corresponds to the change in magnetization of $5.8 \times 10^{14}\ \beta/cm^3$, and the value of the left hand side of Eq.(7) is 0.0064. When we take $N(D^O) = 9.0 \times 10^{16}\ P/cm^3$, $H_O = 750$

G, T_L=1.6 K, the polarization factor $\beta H_o/kT_L$ is 0.032 and the magnetic moment of the D^- state in Bohr magneton unit β, $H_o/((m^*/m_o)^2 E(D^-))$ is 0.064 in our experimental conditions. The D^- state is assumed to be isolated for simplicity.

First, if the PM signal observed is attributed only to the first term in the right hand side of Eq.(7), T_s is estimated to be 1.97 K, which corresponds to the relative rise of 23 % from T_L.

Next, if the signal is attributed only to the second term, i.e., the diamagnetism of the D^- state, the ratio $N(D^-)/N(D^o)$ is estimated to be 9.4 %. In the previous work,[33-35] the electron capture cross section of a neutral donor D^o and that of an ionized donor D^+ were studied. The former is of the order of $\pi R(D^o)^2$,i.e., the area of the 1s ground state of the neutral donor. The latter is two orders of magnitude larger than the cross section of the neutral donor, because a conduction electron is initially trapped in a higher excited donor state with a large electron orbit and subsequently relaxes to the ground state via lower excited states. The concentrations of the D^- and D^+ should be equal in the uncompensated sample. Therefore the ratio $N(D^-)/N(D^o)$ should be smaller than the ratio of the capture cross section of D^o to that of D^+, which is inconsistent with the experimental value of 9.4 % estimated above. In the concentration region above 1 x 10^{16} P/cm^3, however, the D_n^- compleces are formed and their electron orbit is expected to be larger than the isolated D^- state. This larger orbit will contribute the larger diamagnetism at a small amount of the D_n^- compleces and may decrease the difference between experiment and theory.

On the other hand the experimental fact that the PM signal is absent in the p-type sample cannot be undrestood from the origin of the orbital diamagnetism, because the corresponding A^+ state should be produced by the IR illumination in the p-type sample and the diamagnetism of the A^+ state is the same order in magnitude as that of the D^- state[36]. In addition the fact that the PM signal amplitude increases under the FIR illumination cannot be understood from the diamagnetism of the D^- states. The above discussions suggest that the diamagnetism of the D^- states is less possible for the PM effect, but we have no positive evidence to ascribe the PM effect to the spin depolarization of the neutral donors.

Finally we summarize the experimental results of the PM effect on Si as follows.

(1) The PM signal is observed only in the n-type and uncompensated samples.

(2) The half-decay time of the signal depends on the temperature, the donor concentration and the IRBG intensity. The increase in the relaxation rate is proportional to the photocarrier concentration.

(3) The signal amplitude is not proportional to the excitation intensity, and depends on the BG intensity, the donor concentration and the temperature.

(4) The origin of the PM effect is attributed to either the depolarization of the donor spins or the orbital diamagnetism of the D^- state.

The crucial experiment on the origin of the PM effect will be

presented in ChapterⅣ .

(5) The FIR light illumination increases the signal amplitude contrary to the prediction based on the orbital diamagnetism of the D^- states.

ChapterⅣ . SQUID-ESR on Shallow Donors in Si

The SQUID-ESR gives direct information on the spin reversal of the donor electrons and their spin-lattice relaxation. The experimental results are compared with the PM effects to clarify the origin of the PM effects.

The instruments were almost the same as used in ChapterⅡ .2, and a change in magnetization induced by the ESR saturation was observed. Besides, the cross effect of the PM effect and the ESR saturation was examined. On sample 9-16 P(C) the ESR spectrum and the spin-lattice relaxation were observed under illumination of the IRBG light. In these measurements, the IRBG light and the IR exciting light are introduced onto the sample through the quartz plunger in the coaxial cavity shown in Fig. 8. The IR source is a tungsten lamp for both of the BG and exciting lights. The intrinsic light was cut off by a Si thin plate, and the remaining light was guided to the sample through the glass fibers. The wavelength of the BG light is ranging from 1 to 1.5 μ m.

1. Experimental Results

1-1. ESR Spectrum

The ESR spectra for samples 9-16 P, 9-16 P(C), and 1.5-17 P were observed at 440 G and at 4.2 K or around 1.7 K. The results are shown in Fig. 20. The ESR spectrum of phosphorus doped Si consists of a doublet, called A_1 line,[4] which is separated by 117 MHz due to the hyperfine interaction between a donor electron and P^{31} nucleus. Since the tunable range of the cavity frequency is about 100 MHz in our method, only one of the A_1 lines is observed. At the center of the two A_1 lines, a broad central peak, which is called A_o line, is observed for all the samples used.

For sample 9-16 P(C), it was found that the BG light considerably influences the spectrum. In the presence of the IRBG light, the height of the A_1 line is increased for the same microwave intensity and the linewidth is narrowed as illustrated in Fig. 20.

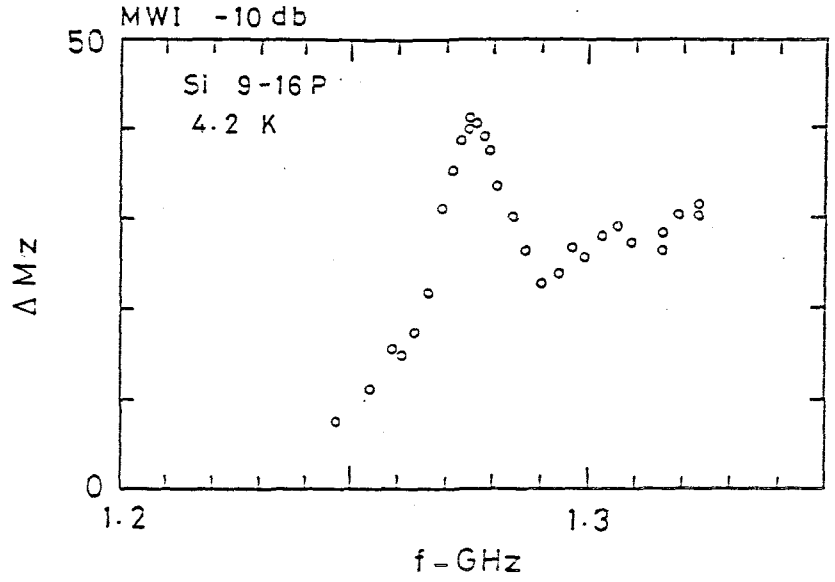
MWI -10 db
50
Si 9-16 P
4.2 K
ΔMz
0
1.2
1.3
f-GHz

(a)

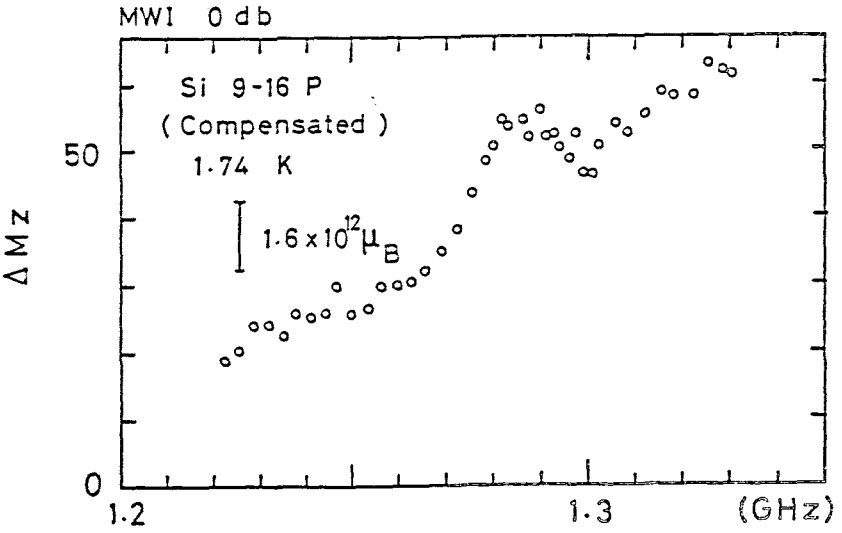
MWI 0 db
Si 9-16 P
(Compensated)
1.74 K
50
1.6x10^12 μB
ΔMz
0
1.2
1.3
(GHz)

(b)

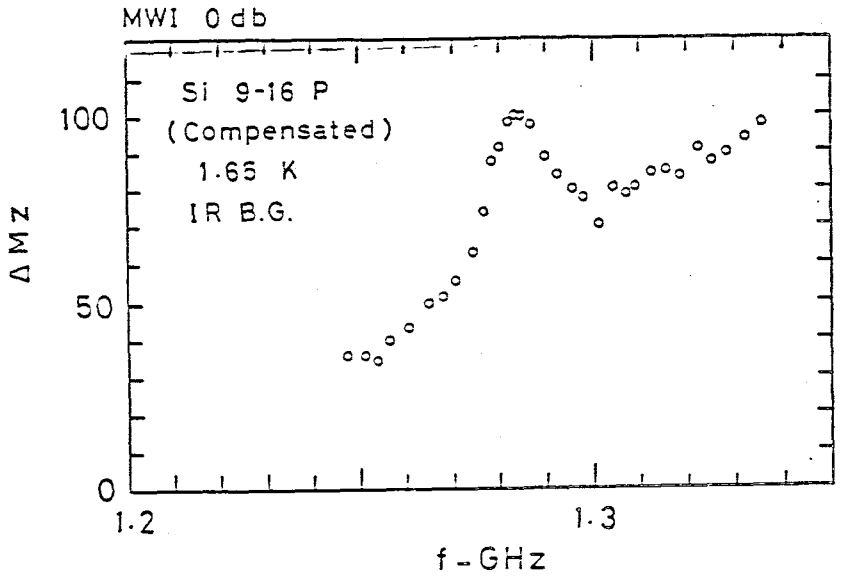

(c)

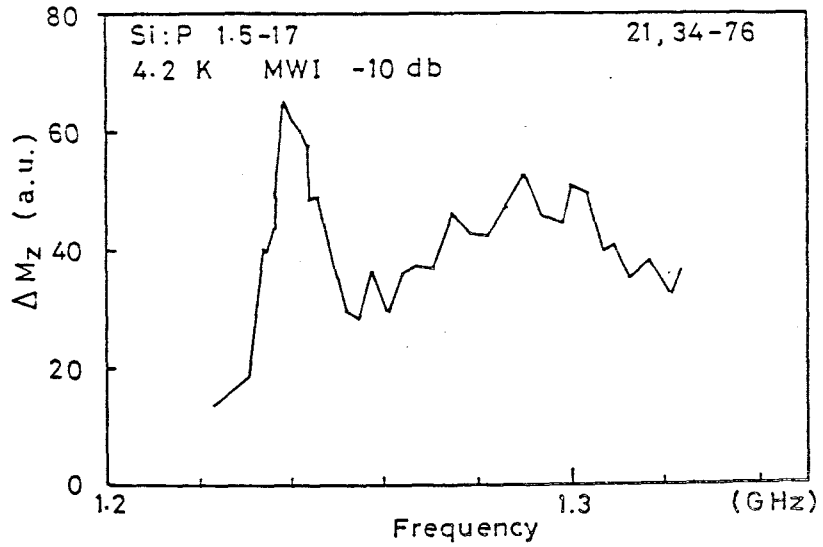

(d)

Fig. 20

Difference in the observed ESR lineshapes of phosphorus doped Si. The measurements were made on one of the hyperfine doublet at 440G.

(a) uncompensated sample 9-16 P at 4.2 K without BG light

(b) compensated sample 9-16 P(C) without BG radiation at 1.65 K

(c) the same sample as (b) with BG radiation.

(d) uncompensated sample 1.5-17 P without BG light.

The dependence of Δ Mz on microwave intensity was observed for each sample. The saturated values of Δ Mz are shown in **Table 4.** In the absence of the BG light sample 9-16 P(C) shows the saturated value of one half of the uncompensated sample 9-16 P, which agrees well with the decrease in the neutral donor concentration by compensation as mentioned in ChapterⅢ .1. In the presence of the BG light the saturated value of Δ Mz is increased to 1.7 times its dark value., which indicates that almost all of electrons trapped by divacancies, V_2^-, are transferred to ionized donors by the BG light and consequently the number of neutral donors returns to that before the compensation.

Table 4

The spin-lattice relaxation time T_1 and the saturated value of Δ Mz expressed by the SQUID output voltage for phosphorus doped samples. Microwave power employed is 10 dbm.

SAMPLE	TEMP.	Δ Mz	T_1 (msec) (FITTING VALUE)
9-16 P	4.2 K	0.33 V	1200
9-16 P	1.66 K	0.97 V	2610
9-16 P with IRBG	1.66 K	0.86 V	240
9-16 P(C)	1.62 K	0.44 V	1420
9-16 P(C) with IRBG	1.62 K	0.73 V	850
1.5-17 P	1.77 K	1.49 V	40

1-2. Spin-Lattice Relaxation Time

The decay curves after the ESR saturation with and without the BG light were observed for each sample at the center of the A_1 peak. These measurements lead to information on the spin lattice relaxation of neutral donors and its change induced by the IRBG light.

The decay curve on sample 9-16 P is shown in Fig. 21-(a). The observed spin lattice relaxation times, T_1, for samples 9-16 P and 1.5- 17 P are consistent with the previous result of Feher et.al.[2] as shown in Table 4. In the present study, the relaxation times are obtained from the slope of the semilogarithmic plot of the decay curve using the least mean square fitting. The decay curve is not simply exponential as shown in Fig. 21-(a) and an initial fast decay component appears. The present observation is the first time to measure T_1 by the transient decay curve of magnetization for shallow donors in Si.

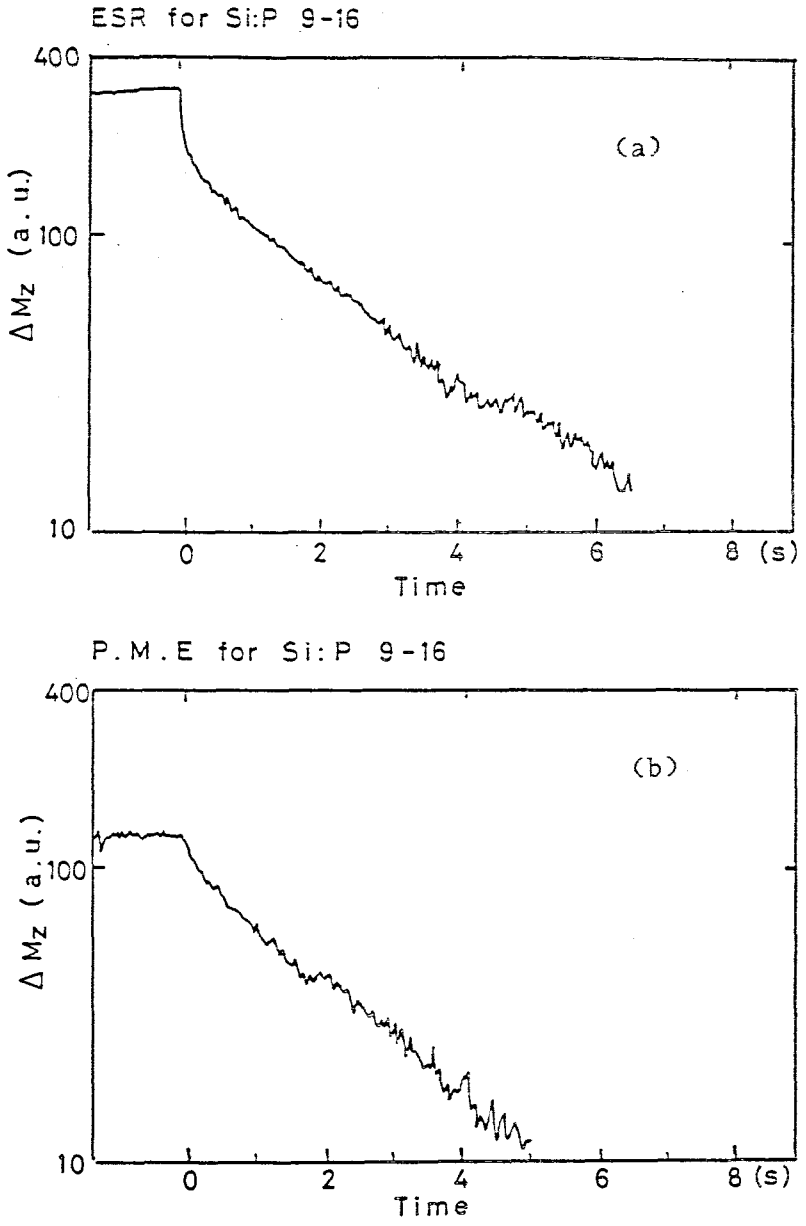

Fig. 21

Comparison of the decay curves between the SQUID-ESR and the PM measurements on the sample 9-16 P at 1.79 K and at 440 G. The decay curves are drawn in the semilogarithmic plot.

(a) SQUID-ESR measurement on sample 9-16 P. The slope gives the relaxation time of 2.3 sec. The microwave power is 10 dbm.

(b) PM measurement. The slope gives 2.1 sec. The excitation is made using the tungsten lamp with the glass filter.

The fast decay component is larger in (a) than in (b).

Similar to the PM measurement the BG light effect was observed for various donor concentrations. As shown in Fig. 15, sample 9-16 P shows the increase in the relaxation rate proportional to the TLBG intensity g_o^* and sample 1.5-17 P shows no dependence on the BG intensity. These results are quite similar to those of the PM effect. On the other hand the sample 9-16 P(C) is less dependent on g_o^* than the uncompensated sample 9-16 P. The decay curve of the sample 9-16 P(C) shown in Fig. 22 has the large fast decay component. Here the spin-lattice relaxation time is obtained from the slower decay component. In the presence of the BG light the ratio of the fast decay component to the total signal amplitude is decreased by the BG light. The spin lattice relaxation times of the compensated sample are listed in Table. 4.

1-3. Correlation between the ESR and the PM Effect

It has been examined whether the PM signal includes the contribution of donor spins or not. The PM signal almost disappears for sample 9-16 P when the donor spins is depolarized by the ESR saturation. This result verifies that the observed PM effect is the change in the polarization of donor spins as discussed later.

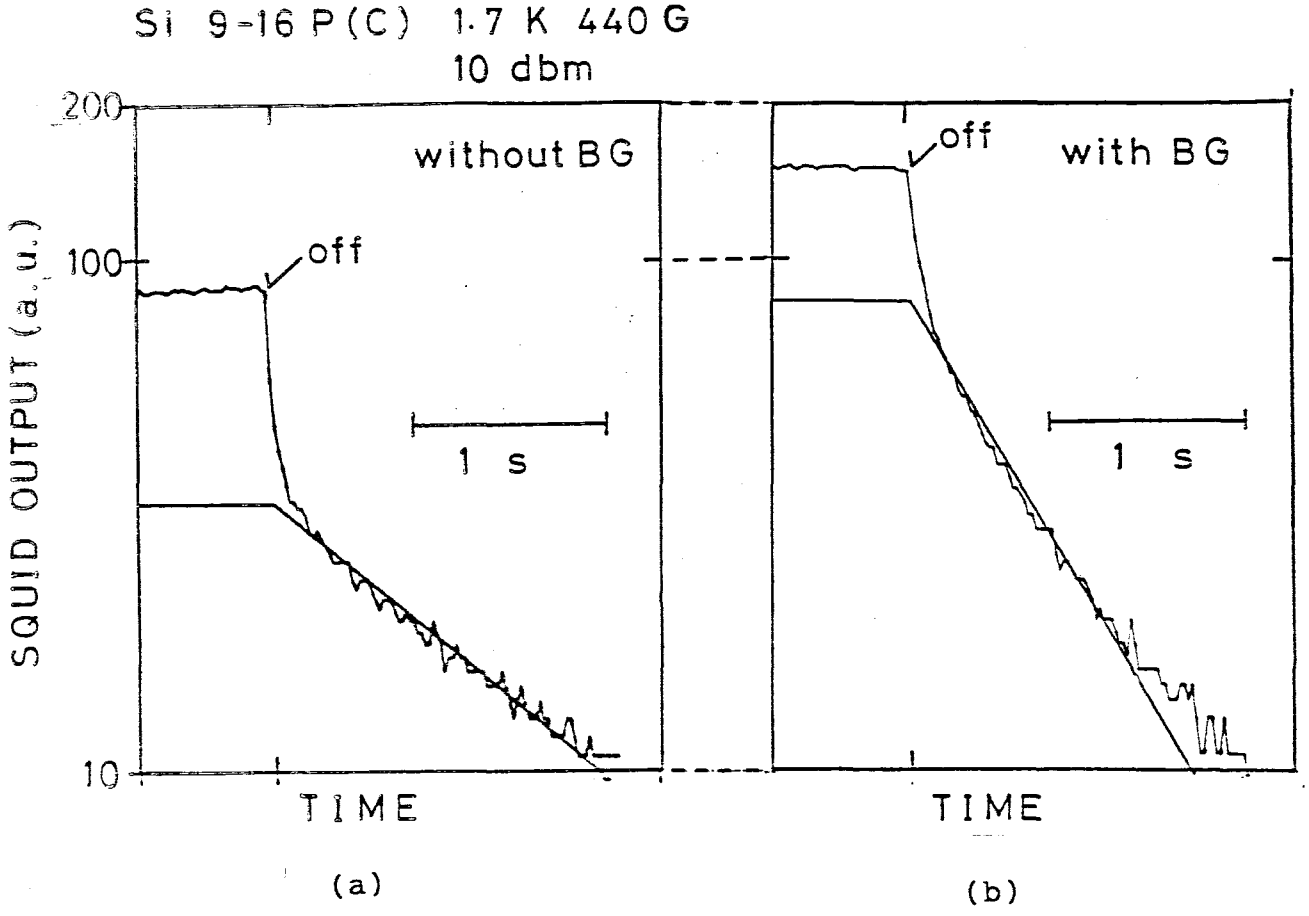

Fig. 22

Comparison of the decay curves after the ESR saturation with and without BG light at 1.7K and 440G on sample 9-16 P(C). Microwave power is 10dbm.

(a) without IR BG

(b) with IR BG

The solid straight lines denote the fitted curve. The relaxation time is 1.4 sec and 0.85 sec for (a) and (b), respectively. The fraction of the fast decay component to the total amplitude is larger in (a) than in (b).

2. Discussion and Summary

The most important purpose of the SQUID-ESR measurement is to identify the origin of the PM effects described in Chapter Ⅲ. We mentioned two possibilities in ChapterⅢ-3: the depolarization in the donor spins and the diamagnetism of the D^- state. In our experiment the static magnetic field is weak and the polarization factor $\beta H/kT$ is about 0.03 at 1.7 K and at 400 G. In the case of $\beta H/kT \ll 1$, the generation of the D^- states should be independent of the spin depolarization. The fact that the PM signal disappears by the ESR saturation described in ChapterⅣ.1-3 indicates that the PM effect is not due to the orbital diamagnetism of the D^- state but due to the spin depolarization of the donors. In addition, in Fig. 21, the two curves of the PM signal and the SQUID-ESR signal is quite similar, though the latter has the larger fast decay component. Consequently we conclude that the steady state amplitude of the PM signal and the half-decay time represent the decrease in the spin polarization and the spin-lattice relaxation time of the neutral donors, respectively.

In below we present some notable results and discuss them. The influence of the BG light on the spin-lattice relaxation time will discussed in ChapterⅥ.

Concerning the compensation effects, it was reported that the relaxation time is shortened by compensation, which agrees with our result shown in Table 4 without IRBG light. The decrease in T_1 was explained by the spin reversal associated with the hopping motion of the donor electron to unoccupied donor sites . When the IRBG light($h\nu = 1 \sim 1.5 \mu$ m) is illuminated on the sample,

the electrons released from the deep centers V_2^- are transferred to ionized donors D^+ owing to the difference of the optical absorption, and consequently the number of the neutral donors is increased up to the original uncompensated value. Therefore the saturated value of Δ Mz is increased to that of the uncompensated sample as shown in Table 4. No reports have been found on the decay form and on the BG effect of the relaxation time for the compensated sample. Compensation produces the fast decay component and the broadening of the A_1 line in the SQUID-ESR. This result may be due to an internal electric field arising from ionized centers such as D^+ and V_2^-. In the presence of the BG light the internal electric field will disappear owing to the neutralization of the charged centers as mentioned above. Accordingly the fast decay component is reduced and the A_1 line is narrowed by the BG light.

In summary, the SQUID-ESR measurement on phosphorus doped Si has been performed for the determination of the origin of the PM effect. The PM signal vanishes under the ESR saturation. The decay curves are almost the same between the PM and SQUID-ESR measurements. The effect of the IRBG light on the spin-lattice relaxation time is quite similar to that of the half decay time of the PM signal. Hence we conclude that the PM effect is due to the depolarization of the donor spins.

ChapterV Far-Infrared Photoconductivity

1. Experimental Arrangement

Figure 23 shows the experimental arrangement for the measurement of photoconductivity. We measured the change in voltage across resistance R_o, ΔV, with and without the photoexcitation. The FIR source is the gas laser which is pumped by a CO_2 laser. The laser wavelengths used are 170 μm (CH_3OH) and 393 μm (HCOOH). The IR source for generation of the D^- states is a tungsten lamp or the room temperature radiation. The cold filters are used for diminishing the background radiation from the room temperature environment. The characteristics of the filters were already shown in Table 2.

The samples are 9-16 P and 3.2-17 P. The electrodes are formed on the chemically etched sample using a ultrasonic soldering. It is difficult to make the ohmic contact in the low concentration region below 1 x 10^{17} P/cm^3. Our samples showed a slight deviation from the ohmic.

The constant voltage is applied on the sample in the measurement of the transient photoconductivity, in order to eliminate the influence of the capacitance between the electrodes.

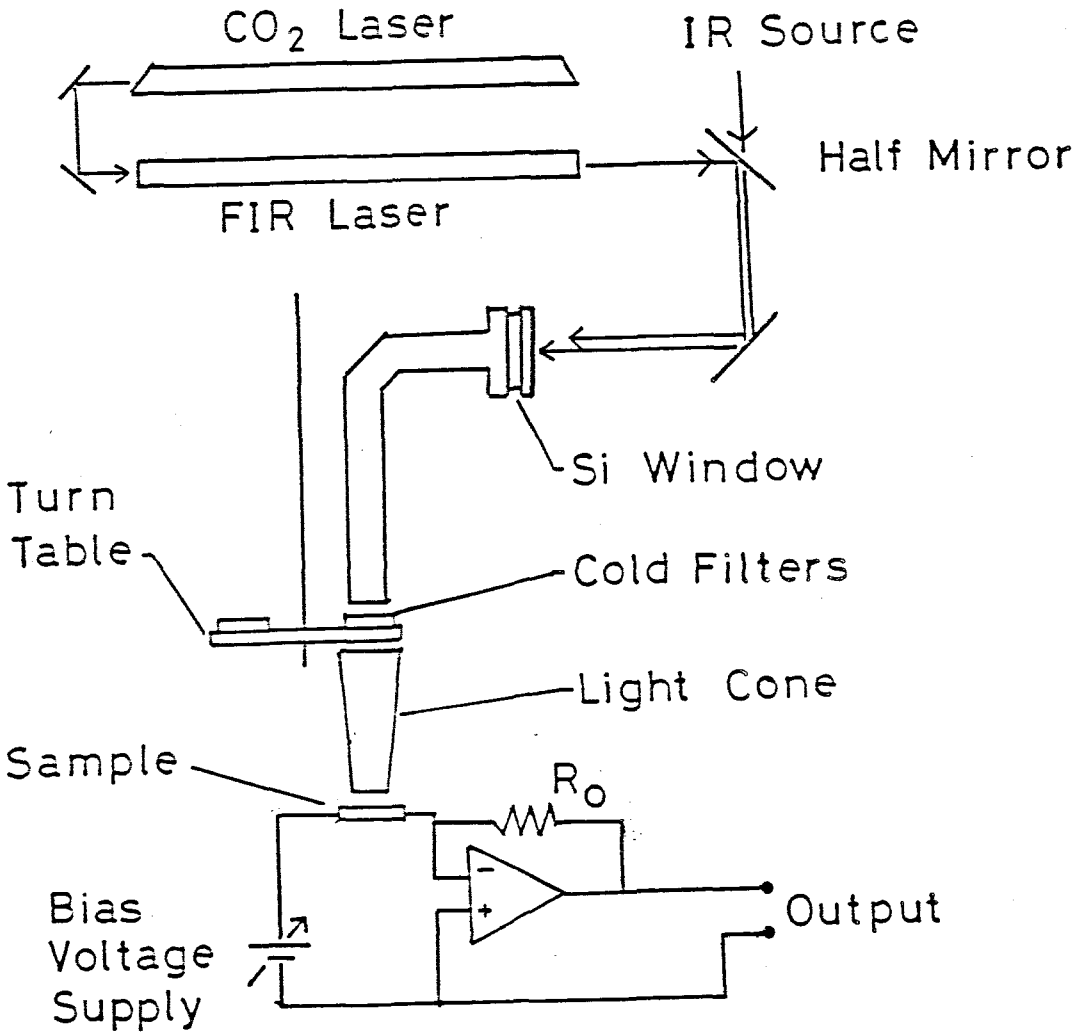

Fig. 23

Experimental arrangement for the FIR photoconductivity measurement. The FIR source is a gas laser pumped by a CO_2 laser. The IR and the FIR lights are superposed at the half mirror of Si and are guided to the light pipe. The cold filters are used to diminish the RTBG light. The constant voltage bias is applied on the sample using an operational amplifier with extremely high input impedence ($\sim 10^{12}\Omega$).

The measurement was made in two modes. In the first mode the IR light is continuously supplied on the sample and the photoconductive response for the chopped FIR light is detected by a lock-in amplifier. In the second mode the FIR light is continuously supplied and the temporal change in photoconductivity is recorded in the digital memory after the pulsed IR light. The first mode is used for measuring the number of the D^- states. The second mode is used for the measurement of the lifetime of the D^- state. In both modes the FIR photocurrent is assumed to be proportional to the D^- concentration.

The IR light intensity shown in Table.2 and .3 is estimated by the measurement of the photoconductive change induced by the illumination of the IR light with the apparatus mentioned above.

2. Experimental Results

The dependence of FIR photocurrent on the IR excitation intensity is shown in Fig. 24, which indicates the saturation of the D^- concentration. The difference due to the FIR wavelength was not observed. The maximum FIR photocurrent observed is about 1 % of the IR photocurrent.

Next, the lifetime of the D^- state is measured in the same way as Norton's work.[11] After the pulsed IR excitation the conduction electrons are trapped by the ionized donors in the order of 10^{-9} sec, and we observe a corresponding fast decay with a dominant amplitude. In addition, we also observe a small and slow tail in the presence of the continuous FIR illumination as shown in Fig. 25. The tail is attributed to the decay of the D^- state. When the Al_2O_3 filter is used, the tail is observed without the FIR laser light, which may be due to the FIR component of the room temperature radiation. With increasing the FIR laser intensity, the amplitude in the tail part is increased correspondingly.

The decay time in the tail is about 2.5 msec at 1.7 K, and is not affected by the irradiation of FIR light. The relaxation time is longer than the value 0.5 msec obtained by Norton who used a sample with 8.5×10^{15} P/cm^3. The difference in the relaxation time between samples 9-16 P and 3.2-17 P has not been observed in our measurement.

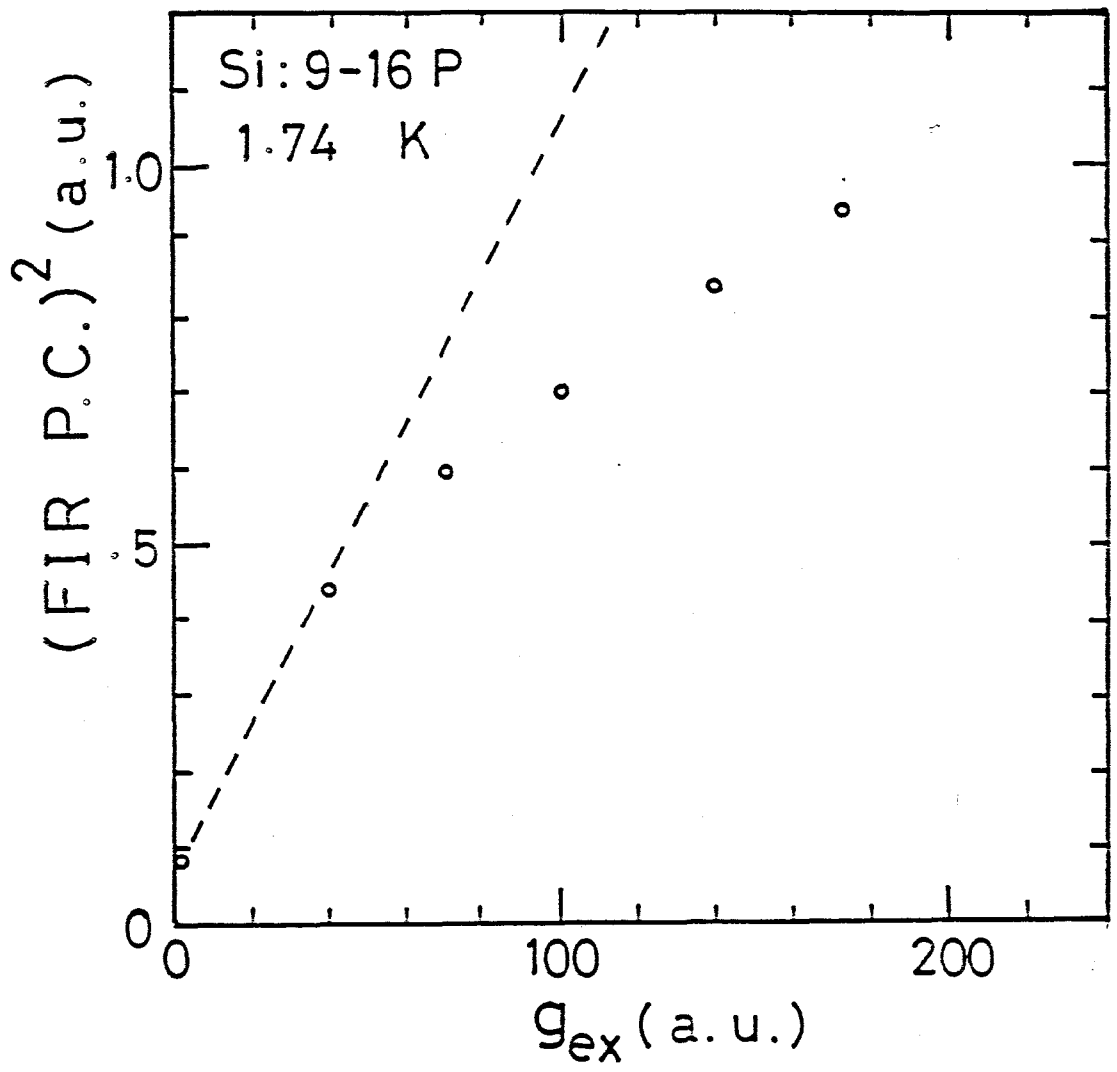

Fig. 24

FIR photocurrent versus the IR excitation intensity g_{ex}. The FIR light is chopped and the IR light is illuminated continuously. The IR source is the tungsten lamp, FIR line is 170μm. The bias voltage is 30V. The ordinate indicates square of the amplitude of the photoconductive signal synchronized to the chopped FIR light. Theory predicts the density of the D^- states to be proportional to the square root of g_{ex} according to Eq.(9) (See text).

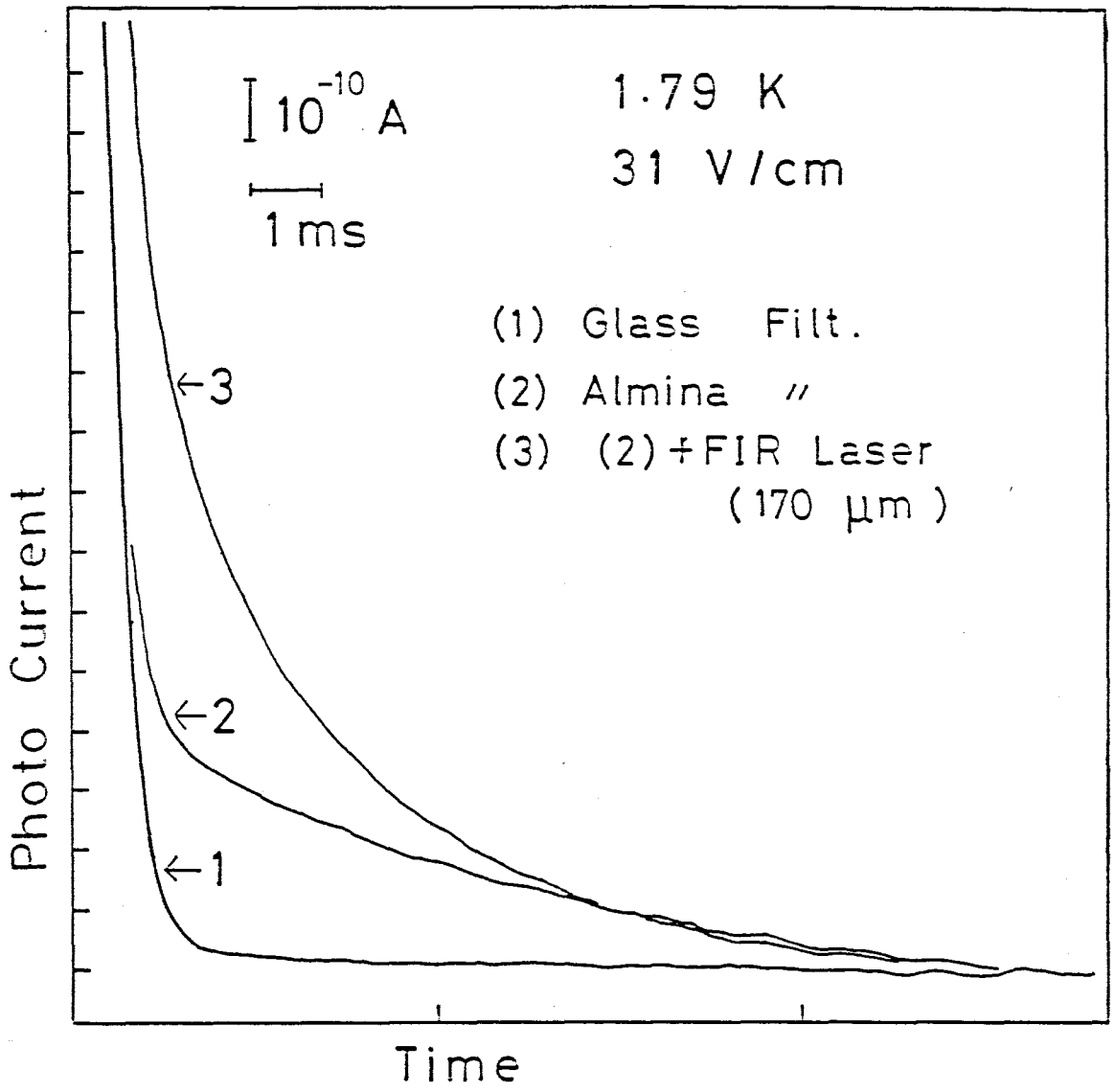

Fig. 25

The tail part of the decay curve of photoconductivity after the pulsed IR excitation at 1.79 K for sample 9-16 P. The FIR light from the room temperature environment or the FIR laser is illuminated continuously. The integers denotes defference in the FIR intensity. No 1 denotes the glass filter which cuts the FIR light off completely. No 2 denotes the Al_2O_3 filter which is transparent in the FIR region of the RT radiation. In No 3, a FIR light is applied on the sample through the Al_2O_3 filter. The bias voltage is 30V.

3. Discussion and Summary

The recombination of the D^- electron with the D^+ state is considered to occur in two ways: by excitation to the conduction band and subsequent transfer to the recombination center D^+, or by hopping via neutral donors. At a liquid helium temperature the thermal excitation to the conduction band can be neglected, and the room temperature FIR light reaches the sample. When the additional FIR laser light is illuminated on the sample, the lifetime of the D^- state is not reduced as shown in Fig. 25. Therefore we conclude that the most dominant recombination process is due to the hopping. The lifetime of the D^- state due to the hopping is much longer than that of the conduction electron. After the IR excitation is turned off, a part of photocarriers are captured by theionized donors in a very short time, and the decay of the D^- states proceeds slowly. In the presence of the FIR light this slow decay is observed as the decay of the photocurrent. Hence the slow tail shown in Fig. 25 is due to the hopping process of the D^- electrons.

Next, we assume the rate equation as follows:

$$\frac{d}{dt}N(D^-) = g_{ex} - \gamma\, N(D^-)^2 \quad , \qquad (8)$$

where g_{ex} is the generating rate of D^- state and γ the recombination constant of D^- and D^+ state. We assume that $N(D^-)=N(D^+)$, for the uncompensated samples. Since the D^- states

are generated by the capture of the conduction electron by neutral donors, we use the same symbol g_{ex} as used in ChapterⅢ. Here we neglect the excitation of the D^- electron to the conduction band induced thermally or by the FIR light, namely, the recombination occurs only by hopping.

The steady state solution of Eq.(8) gives the dependence of $N(D^-)$ on the excitation intensity g_{ex} as follows:

$$N(D^-) = (g_{ex} / \gamma)^{1/2} \quad . \qquad (9)$$

Equation (9) is compared with the experimental result shown in Fig. 24. The fitting result is not satisfactory. With increasing g_{ex} the experimental points deviates from the linear line. In other words, the saturation behavior appears more strongly than the predicted by Eq.(9). This result suggests that the generation of the D^- state is suppressed with increasing the D^- concentration. The recombination by the hopping may be accelerated by the Coulomb attractive potential of the D^+ centers, and the recombination constant γ may be increased with increasing D^+ concentration. As a consequence, $N(D^-)$ is decreased compared to the expected value with increasing g_{ex}.

The decay curve obtained from the time dependent solution of Eq.(8) is not exponential but a hyperbola. However we cannot decide strictly whether the tail part of the decay curve shown in Fig.25 is a hyperbola or exponential.

The lifetime of the D^- state obtained here is longer than the previous value. In our sample the D_n^- compleces are expected to be formed, because our sample contains the donors with higher

concentration. The D_n^- compleces have larger binding energy than the isolated D^- state and therefore may have longer lifetime.

In summary the lifetime of the D^- state has been obtained from the decay of the FIR photoconductivity and is 2.5 msec. This value is somewhat longer than the previously obtained (a few hundreds micro-seconds) but it may be ascribed to the nature of the D_n^- compleces. The fact that this lifetime is quite different from the half-decay time of the PM signal indicates that the PM signal is not due to the orbital diamagnetism of the D^- states.

ChapterVI . Discussion

First we summarize the observed results which should be discussed. In ChapterIII it is presented that the PM effect is induced by an unpolarized light and is associated with shallow donors. Two possibilities are considered as the origin of the PM effects: the depolarization of the donor spins or the orbital diamagnetism of the D^- states. In ChapterIV it is presented that the decay form and the decay time after the ESR saturation are quite similar to those of the PM signal after the photo-excitation, and the PM signal disappears under the ESR saturation. Therefore it is concluded that the PM effect is not due to the diamagnetism of the D^- state but due to the depolarization of the donor spins. In addition the photoconductivity measurement indicates that the lifetime of the D^- state is of the order of 10^{-3} sec which is much shorter than the half-decay time of the PM signal. Accordingly the possibility of the PM effect due to the diamagnetism of the D^- states is excluded. The half decay time $\tau_{1/2}$ is equivalent to the spin-lattice relaxation time, and agrees well with the relaxation time reported before[2], except for sample 2.2-16 P. For sample 2.2-16 P an extremely long T_1 of about 10^3 sec was reported at 1.25 K and at 750 G, while T_1 observed here is about 1 sec at 1.6 K and at 750 G. The possibility for difference of the relaxation times may be due to the inevitable weak BG light illuminated on the sample in our case. Since the low doped sample has a long T_1, even the weak BG light may appreciably reduce the relaxation time. The apparatus for the PM measurement has the window for

the incoming light, and hence such a weak BG light may reach the sample. The SQUID-ESR measurement under the strictly dark condition will give a longer relaxation time. This is a future problem.

Next we present the problems which should be elucidated in this chapter. The PM effect observed on shallow donors in Si reveals two events. One is the decrease in the spin-lattice relaxation time of the donors induced by the IR BG light. This phenomenon was already pointed out by Feher et.al.[2]. Another is the depolarization of the donor spins induced by the IR light. This phenomenon has not been reported before.

1. BG Effect on the Relaxation Time

Empirically the dependence of the half-decay time $\tau_{1/2}$ on the BG intensity g_o^* is deduced from the result shown in Fig. 15, and the relation of $\tau_{1/2}$ to g_o and g_o^* is as follows:

$$\frac{1}{\tau_{1/2}} = C_3 (g_o + g_o^*) + \frac{1}{\tau_{1/2^o}} , \qquad (10)$$

where g_o the RTBG light intensity, g_o^* the TLBG light intensity, $\tau_{1/2}$ the spin-lattice relaxation time, $\tau_{1/2^o}$ the value in dark, C_3 the fitting parameter independent of the BG intensity. The RTBG intensity is controlled to some extent by the choice of the cold filters used. The total BG intensity applied on the sample is the sum of the TLBG intensity g_o^* and the RTBG intensity g_o as

given by the first term in the right hand side of Eq.(10).

The value in dark $\tau_{1/2}^{o}$ results from two mechanisms: one is the spin-lattice relaxation time due to the coupling of the donor spin with the lattice, which has been studied by several workers before, and another is due to the interaction between the donor spins. In the concentration region above 1 x 10^{16} P/cm^3 Feher et.al. found that the relaxation time rapidly decreases with increasing the concentration owing to the latter mechanism. In our experiment the similar concentration dependence is obtained as shown in Fig. 16. The temperature dependence indicates that the direct phonon process is dominant at low temperatures below 2 K, and the Raman process contributes to the relaxation with increasing temperature.[2] In Fig. 14 T_1 varies as $T^{-1.7}$ for the weakest BG intensity (with Al_2O_3 filter), which does not agree with the previous result mentioned above. The reason of this disagreement is not understood yet.

On the other hand it was also pointed out that the rate T_1^{-1} is increased proportionally to the carrier concentration as described by Eq.(10). The value of g_o^* is estimated from the photoconductance in this work, and therefore g_o^* denotes a quantity proportional to the photoexcited carrier concentration as long as the mobility of the carrier is assumed to be independent of the light illumunation. For the decrease in T_1 with increasing the light intensity, Feher proposed the spin-exchange scattering of the conduction electrons by the neutral donors[2]: The spin-lattice relaxation of the donors occurs through the bottleneck of that of conduction electrons. Since the spin-lattice relaxation time of the conduction electrons, T_{1c}, is of the order

of 10^{-7} sec, a small amount of conduction electrons increase the relaxation rate. In Appendix, the relation between T_1 and quantities T_{1c} and n_e is given in Eq.(A-4) or (A-5). Since the observed value of T_1 in the presence of the BG light in sample 9-16 P is 0.24 sec, the corresponding value of n_e is of the order of 10^{10} electrons/cm^3, which may be too large.

In Fig. 15 the experimental points denoted by No 3 are obtained using a quartz filter, i.e., nearly $g_o=0$. In the presence of the RTBG light(No.1 and 2), i.e., $g_o \neq 0$, the value of the relaxation rate at $g_o^*=0$ is shifted upward owing to nonzero of g_o. The fact that the lines 1 to 3 in Fig. 15 appears nearly parallel agrees with that C_3 is independent of the BG intensities, g_o and g_o^*. The relaxation rate obtained by the SQUID-ESR measurement on the same sample as the PM one is denoted by No 4. The lines 3 and 4 are in good agreement in their slope though the absolute values differ slightly. This difference is trivial because it arises from the difference between the half-decay time and the 1/e decay time.

Using Eq.(10), the temperature dependence and the donor concentration dependence of $\tau_{1/2}$ can be explained. In below we consider only the case of $g_o^*=0$. The temperature dependence of $\tau_{1/2}$ disappears with increasing the BG intensity as shown in Fig.14. In Eq.(10), in the case of a large g_o where the first term is much larger than the second term, the second term does not contribute to $\tau_{1/2}$. Provided C_3 is independent of the temperature, the temperature dependence of $\tau_{1/2}^o$ disappears for the strong BG intensity. In contrast, with increasing the donor concentration, the second term in Eq.(10) becomes much larger

than the first term, and therefore the BG light does not affect the half-decay time for the sample with the concentration above 1.5×10^{17} P/cm^3 as shown in Fig. 16.

2. Rate Equation Approximation

Another empirical equation is introduced to explain the dependence of the signal amplitude A_{ex} on the excitation intensity g_{ex} shown in Fig .17. In the absence of the BG light, the rate equation for the spin magnetization under the photo-excitation is assumed to be

$$\frac{d\,\Delta Mz(t)}{dt} = C_4\, g_{ex} - \frac{\Delta Mz(t)}{T_1} \quad , \qquad (11)$$

and

$$\frac{1}{T_1} = C_3\, g_{ex} + \frac{1}{T_1{}^{o}} \quad , \qquad (12)$$

where $\Delta Mz(t)$ is a decrease in Mz from its thermal equilibrium value, g_{ex} the density of photo-electrons, T_1 the spin-lattice relaxation time, $T_1{}^{o}$ the dark value of T_1, and C_4 the fitting parameter. In Eq.(11) the positive sign of $\Delta Mz(t)$ means the diamagnetic change.

We assume that ΔMz only arises from the spin reversal of the donor electrons, and neglect the direct contribution of the spin magnetization of the photo-electrons, because the density of the electrons is much smaller than that of the donor spins. However in the first term of the right hand side of Eq.(11), the gener-

ating rate of the depolarization of the donor spins is assumed to be induced by the spin-exchange scattering of photo-elecrons at the donors, and therefore will be proportional to the photo-electron concentration. Since the donor electrons are excited far above the conduction band minima by the IR light, the photo-excited electrons are in a high electron temperature, i.e., a hot electron state. The high electron temperature will lead to the rise in the spin temperature of the photo-electrons which induces the depolarization of the donor spins through the spin exchange scattering. The derivation of Eq.(11) is explained in Appendix. Equation (12) indicates that the relaxation time is decreased by the exciting light, which is essentially the same as Eq.(10). The BG intensity g_o is replaced by the exciting light intensity g_{ex}. In Eq.(12) T_1 means the 1/e decay time, and in Eq.(10) $\tau_{1/2}$ the half-decay time, and therefore the difference between T_1 and $\tau_{1/2}$ is only a constant factor.

The signal amplitude A_{ex} is equal to the steady state solution of Δ Mz except for a proportional factor. The steady state solution of Eqs.(11) and (12) during the excitation, gives the relation as

$$A_{ex}^{-1} = C_1 + C_2 g_{ex}^{-1} , \qquad (13)$$

where

$$C_1 = C_3/C_4 \quad \text{and} \quad C_2 = (C_4 T_1^{o})^{-1} . \qquad (14)$$

In the presence of the BG light with the intensity g_o, we must replace $(T_1^{o})^{-1}$ by $[C_3 g_o + (T_1^{o})^{-1}]$, and g_{ex} by $(g_{ex} + g_o)$

in Eqs.(11) and (12). The steady state signal amplitude A_{ex} is the difference between Δ Mz with and without excitation denoted by g_{ex}. Consequently, Eq.(13) is still valid, though C_1 and C_2 is replaced as follows:

$$C_1 = (C_3 / C_4) (1 + C_3 T_1^{o} g_o) ,$$

and (15)

$$C_2 = (C_4 T_1^{o})^{-1} (1 + C_3 T_1^{o} g_o)^2 .$$

The solid lines in Fig. 17 are obtained using Eq.(13) together with Eqs.(14) and (15), and agreement with the experimental results is satisfactory. In addition, Eq.(15) predicts that the quantity C_1^2/C_2 is independent of the BG intensity. In the absence of BG light (glass filt.) and in the presence of BG light (no filt.), the quantities C_1^2/C_2 are obtained to be 0.073 and 0.064 from the fitting result in Fig. 17, respectively. This small difference is regarded to be nearly consistent with the independence of the BG intensity.

The donor concentration dependence of A_{ex} is explained qualitatively by Eqs.(13) and (14). In Eq.(13), the second term in the right hand side is proportional to the product of T_1^{o} and g_{ex}, and is more dominant than the first term. With increasing donor concentration the photo-electron density g_{ex} is increased because the absorption coefficient of the photo-ionization of the donors is increased, while the spin-lattice relaxation time T_1^{o} is decreased. Hence we expect the maximum of A_{ex} for an appropriate donor concentration.

The time dependent solution of Eq.(11) is described by an ex-

ponential function. The observed decay curve, however, is not exponential as shown in Fig. 21, which may be attributed to a spatial distribution of spin-lattice relaxation time due to inhomogeneity of the donor concentration in the sample. The spin-lattice relaxation rate in the absence of the BG light depends on the interaction between the donors. In fact in the donor concentration region of our samples, the spin-lattice relaxation times are strongly dependent on the concentration, and therefore a slight fluctuation in the concentration will induce the appreciable distribution in the spin lattice relaxation time. This assumption enables us to understand the fact that the fast decay component is smaller in the PM signal than in the ESR as shown in Fig. 21. The PM signal amplitude is decreased with decreasing the relaxation time as indicated by Eqs.(13) and (14). Accordingly the part of the sample with the shorter spin-lattice relaxation time produces the smaller signal than the part of the sample with the longer relaxation time. Thus the relation of Eqs.(10) to (15) well describes the observed results of the PM effect.

3.Other Problems

(1) The absence of the PM signal in the p-type sample is explained as follows. The ESR spectrum on the p-type sample cannot be observed in the absence of uniaxial stress owing to the internal random strain, which indicates that the hole strongly couples to the lattice. Accordingly the spin lattice relaxation time is expected to be very short. Therefore the second term of Eq.(8) is considered to be large for the p-type sample, i.e., the PM signal amplitude is correspondingly small.

(2) The absence of the PM signal in the compensated sample has to be explained by the rate equation. Though the relaxation time is decreased slightly by the compensation, it is not so sufficient as to explain the disappearance of the PM signal. Accordingly this absence cannot be explained in the same way as the p-type sample described in (1). One of important influences of the compensation is to reduce the lifetime of photoexcited carriers owing to recombination with the ionized donors D^+. The reduction in the lifetime leads to the reduction in the number of the carriers, and consequently suppresses the rise in the spin temperature of the donors.

(3) As shown in Sec.Ⅲ-2-4, the FIR light increases the PM signal in the presence of the IR light. This result excludes the possibility that the origin of the PM effect is due to the diamagnetism of the D^- states. Then, how is this result explained by the spin depolarization mechanism ? The FIR light is partially

absorbed by the photoexcited carriers and will raise the electron temperature of the carriers. If the spin depolarization is associated with the hot electrons, the rise in the electron temperature will lead to the increase in the PM signal amplitude. However, the degree of the influence of the FIR light on the electron temperature cannot estimated quantitatively. As a future work to verify the mechanism of the hot electrons, we suggest the following experiment. When the rf electric field, instead of FIR light, is simultaneously applied on the sample with the IR light, the electron temperature of the conduction electron will be raised without a direct heating of the donor spins. Consequently the PM signal will be increased by spin-exchanged inelastic scattering between the donors and the conduction electrons.

(4) Finally we discuss another mechanism on spin polarization of donors in Si. The influence of the compensation was already presented in (2). However we must note another fact accompanied with the reduction in the lifetime of the photoexcited carriers: The formation of the D^- states is disturbed by the exsistence of the ionized centers D^+.

Though the orbital diamagnetism of the D^- state is excluded for the origin of the PM effect, there is no doubt for the photogenerated D^- states in the uncompensated sample. However the total number of the D^- states are too small to yield the observable PM effect. Then, we point out the possibility that a small amount of the D^- states have influence on the polarization of the donor spins. In the concentration region above 1 $x10^{16}$

P/cm^3 the D^- state is not isolated and is expected to form a complex center with several neutral donors, i. e., D_n^-. We assume a model that two neutral donors interact with the same D^- state.(This model can be regarded as D_3^-) Since a D^- state has a closed shell, the superexchange interaction between two donor spins through a D^- state may occur in the presence of photoexcitation. If the interaction is antiferro-magnetic, a pair of antiparallel spins is generated by the D^- state, and the sample magnetization is decreased.

The reduction in the spin relaxation time may also be explained by this model. The superexchange has a spin Hamiltonian of $J\ \mathbf{S}_i \cdot \mathbf{S}_j$, which gives the nondiagonal matrix element between the Zeeman levels.

Since this model is not consistent with the observed result of Δ Mz to be increased by the reduction in the number of the D^- centers as described in Sec. 2-4 of chapterIII , the super exchange mechanism in D_3^- compleces seems to be less possible than the spin exchange scattering mechanism.

Ⅶ Concluding Remarks

(1) The experimental methods for observation of the PM effect and the ESR have been developed in this work using a SQUID magnetometer. Consequently it has been shown that both methods have advantages to obtain the information on the spin-lattice relaxation on ruby and on shallow donors in Si.

(2) As a demonstration of the PM effect and the SQUID-ESR, we present the experimental results on ruby. For 0.01 % ruby, the PM and the SQUID-ESR measurements give a quite similar result. For 0.05 % ruby, however, the results obtained by the two methods show different feature in the waveform and the relaxation time. This difference will be studied in a future work.

(3) On shallow donors in Si we have observed the diamagnetic PM signal in the n-type and uncompensated sample. It has been concluded that the PM signal is due to the depolarization of the donor spins from the following reasons: the close similarity of the waveform of the PM signal to the SQUID-ESR signal, the disappearance of the PM signal under the ESR saturation, and the large difference between the half-decay time of the PM signal and the lifetime of the D^- state obtained by the FIR photoconductivity.

(4) The PM effect on shallow donors in Si includes two events: One is the decrease in the spin-lattice relaxation time due to the IRBG light, and another is the depolarization of the donor spins. These events are explained reasonably by the rate equa-

tion proposed. Though the mechanism for these events have not been understood satisfactorily yet, the following models are assumed: the spin exchange scattering of photoexcited carriers by neutral donors and the superexchange interaction between the neutral donor spins through the D^- states.

Appendix

Derivation of the Rate Equation (11)

We derive the rate equation (11) for the spin polarization of the donor electrons under an exciting light and without BG light. Since the photo-electrons ionized from the neutral donors are in the hot electron state, we assume that the spin temperature of photo-electrons T_{sc} is raised from the lattice temperature T_L through an interaction between the hot carriers, e.g., the spin exchange collision. Because of a fast spin-lattice relaxation time of the conduction electrons, T_{sc} reaches a steady state value T_{sc}^{o} immediately after the light illumination. In consequence of the spin exchange scattering of the photo-electrons at the donor site, the spin temperature of the donor electrons T_s is raised so as to produce a change in donor magnetization. We introduce the quantities x and y which are defined as $\beta H_o/kT_s$ and $\beta H_o/kT_{sc}$, respectively. The rate equations of x and y are as follows:

$$dx/dt = - R_a (x - x_o) - R_{ab} (x - y), \qquad (A-1)$$

$$dy/dt = - R_b (y - y_o) - R_{ba} (y - x), \qquad (A-2)$$

where $x_o = \beta H_o/kT_L$, $Y_o = \beta H_o/kT_{sc}^{o}$, $R_a = T_1^{o-1}$, $R_b = T_{1c}^{-1}$, $R_{ab} = T_{ab}^{-1} = \xi n_e$, $R_{ba} = \xi N(D^o)$, ξ is the rate constant of the simaltaneous flip-flop between the donor spins and the carrier spins via the spin exchange scattering, n_e the carrier

concentration. It is assumed that the carrier spin system has much shorter relaxation time than the donor spin system, i.e., $R_b \gg R_a$, and the carrier spin system is in a steady state during the spin reversal process of the donors, i.e., $dy/dt = 0$. The steady state solution of Eq.(A-2) leads to the relation:

$$y = (R_b y_o + R_{ba} x) / (R_b + R_{ba}). \qquad (A-3)$$

If the conduction electrons strongly couple with the lattice and the phonon bottleneck is the spin exchange mechanism between the conduction electrons and the donors, $R_b \gg R_{ba}$. Therefore Eq.(A-3) becomes to that $y = y_o$, and Eq.(A-1) becomes as follows:

$$d(x - x_o)/dt = R_{ab}(y_o - x_o) - (R_a + R_{ab})(x - x_o) \qquad (A-4)$$

$$= \xi (y_o - x_o)n_e - (1/T_1{}^o + \xi n_e)(x - x_o).$$

Considering the relation that $\Delta Mz=-N(D^o)\beta (x-x_o)$ and $g_{ex} = n_e$, we obtain Eq.(11), where C_3 and C_4 are ξ and $\xi N(D^o)\beta (x_o-y_o)$, respectively.

On the other hand, if the donors and the conduction electrons are strongly coupled and the phonon bottleneck is the spin lattice relaxation of the conduction electrons, $R_{ba} \gg R_b$. Therefore Eq.(A-3) becomes to that $y = x + (R_b/R_{ba})y_o$, and consequently we obtain the equation which has similar formula to Eq.(A-4) as follows:

$$d(x - x_o)/dt = (R_{ab}/R_{ba})R_b(y_o - x_o) - \{R_a + (R_{ab}/R_{ba})R_b\}(x - x_o). \qquad (A\text{-}5)$$

In the same way as above we obtain Eq.(11), where C_3 and C_4 are $1/\{N(D^o)T_{1c}\}$ and $\beta\,(x_o - y_o)/T_{1c}$, respectively.

In either case the generation rate in Eq.(11) is proportional to $(y_o - x_o)$, which does not vanish because the photo-electrons are in the hot electron state, i.e., $T_{sc}{}^o > T_L$.

References

(1) W.Kohn, Solid. St. Phys. vol 5, P257

(2) G. Feher, E. A. Gere, Phys.Rev.114, 1245(1959)

(3) D. K. Wilson, G. Feher, Phys.Rev.124, 1068(1961)

(4) S. Maekawa, J.Phys.Soc.Japan Suppl.21, 574(1966)

(5) A. Honig, E. Stupp, Phys.Rev. Lett.1.275(1958)

(6) M. A. Lampert, Phys.Rev.Lett.1.450(1958)

(7) H. A. Bethe, E. E. Salpter. "Quantum mechanics of one- and two- electron system" (Springer, Berlin, 1957) P146ff

(8) M. Taniguchi, S. Narita, Solid State Commun.20, 131(1976)

(10) P. Norton, Phys.Rev.Lett.37, 164(1976)

(11) P. Norton, Proc.Intern.Conf.Phys.Semicond.,993(1979)

(12) M. Kondo, S. Ochi, Y. Nisida, Proc.of Symp.on Superconductive Quantum Electronics(Tokyo 1983) P49, ed. K. Hara

(13) J. S. Philo, Proc.Natl.Acd.Sci.USA, 74, 2620(1977)

(14) H. Heidrich, P. Mateew, Proc.Intern.Conf.on SQUID, 2nd,Berlin(1980) P519

(15) J. Clarke, Proc.IEEE,61, 8(1973)

(16) J. S. Philo, W. M. Fairbank, Rev.Sci.Instrum.48, 1529(1977)

(17) M. Pelizzone, A. Treyvaud, Appl.Phys.24, 375(1981)

(18) S. E. Nave, P. G. Huray, Rev.Sci.Instrum.51, 591(1980)

(19) M. Cerdonio, C. Cosmelli, G. L. Romani, Rev.Sci. Instrum.47, 1(1976)

(20) A. H. Silver, J. E. Zimmerman, Appl.Phys.Lett, 10, 142(1967)

(21) E. P. Day, Phys.Rev.Lett.28, 540(1972)

(22) R. A. Webb, Rev.Sci.Instrum.48, 1585(1977)

(23) R. V. Chamberlin, L. A. Moberly, O. G. Symko, J.Low Temp.Phys.35, 337(1980)

(24) The Zeeman splitting of the ground state of Cr^{3+} in ruby is given by

$$H = g_{//}\beta HzSz + g_{\perp}\beta (HxSx + HySy) + D[Sz^2 - S(S+1)/3],$$

where $g_{//} = 1.982$, $g_{\perp} = 1.979$, $D = -0.1912\ cm^{-1}$, $S = 3/2$ and β is Bohr magneton. The z axis is taken c-axis. See, G. M. Zverev, A. M. Prokhorov, Sov.Phys.-JETP.7,358(1958)

(26) G. E. Pake, "Paramagnetic Resonance"

(27) J. P. Goldsborough, M. mandel, G. E. Pake, Phys.Rev.Lett.4, 13(1960)

(28) S. Sugano, I. Tsujikawa, J.Phys.Soc.Japan,13,254(1958)

(29) E. B. Tucker, Physical Acoustics.vol.4A, ed. W. P. Mason, (Academic Press, N.Y.,1966)P47

(30) Y. Nisida, J.Phys.Soc.Japan.19,2273(1964)

(31) S.-Y. Feng, N. Bloembergen, Phys.Rev.130,531(1963)

(32) G.D. Watkins, J. W. Corbett, Phys.Rev.19,543(1965)

(33) R. A. Brown, M. L. Burns, Phys.Lett.32A, 513(1970)

(34) P. Norton, T.Braggins, H. Levinstein, Phys.Rev.Lett.30, 488(1973)

(35) D. D. Thornton, A. Honig, Phys.Rev.Lett.30, 909(1973)

(36) N. Sugimoto et.al. Solid State Commun. 30, 385(1979)

(38) M. Kondo, Y. Nisida, Proc. of the 17th Intern. Conf. of the Phys. of Semiconductors(San Francisco, 1984) P.1137

(39) Y. Nisida, M. Kondo, Solid State Phys.18, 151(1983)